공학박사학위논문

원통형 노즐로부터 방사되는 분자간 충돌이 존재하는 분자 유동의 방사 특성 모델

The Analytical Model of the Angular Distribution of the Molecular Flux with Intermolecular Collisions Emitted from a Cylindrical Nozzle

2019 년 2 월

서울대학교 대학원

기계항공공학부

김 도 훈

Ph.D. Dissertation of Mechanical Engineering

The Analytical Model of the Angular Distribution of the Molecular Flux with Intermolecular Collisions Emitted from a Cylindrical Nozzle

The Model of the Angular Distribution for
- Optimization of the Linear Thermal Evaporation -
System

원통형 노즐로부터 방사되는 분자간 충돌이 존재하는 분자 유동의 방사 특성 모델

February 2019

Graduate School of Engineering
Seoul National University
Mechanical Engineering Major

Dohun Kim

Abstract (English)

The linear source of a thermal evaporation system, which consist of a crucible in which to put materials and nozzles as the outlet from which evaporated materials emitted, has been used in manufacture processes of semi-conductors and OLEDs. When the molecules of evaporated materials from the nozzle are deposited onto a substrate, the thickness of the deposited molecules depends on the angular distribution of the emitted molecular flux from the nozzle. The angular distribution of the emitted molecular flux from the nozzle is determined by a design of the nozzle, a type and a density of material. The angular distribution is the one of important elements in optimizing the linear thermal evaporation system for depositing uniform thickness on thin film on a substrate.

Various theoretical methods have been studied in an effort to express the angular distribution of the emitted molecular flux mathematically. According to Knudsen in 1907, the angular distribution of the emitted molecular flux from a cylindrical nozzle, can be expressed in the form of $cos^n(\theta)$. The actual angular distribution of the molecular flux emitted from a nozzle, however, does not precisely match the form of $cos^n(\theta)$ by Knudsen.

There are other methods to express the angular distribution more precisely. One is the conventional analytical model integrating the molecules emitted directly and the molecules reflected onto the inner wall of the nozzle by means of numerical integration. Another method involves the direct simulation of molecules being emitted from the nozzle using a Monte Carlo method. Using these conventional methods can allow one to determine the accurate angular distribution of the emitted molecular flux. However, the conventional analytical method has proposed an analytical model of the angular distribution by the change of nozzle design, but cannot express the change of the angular distribution by the collision between molecules. Because

the method assume there are no collision between molecules due to free molecular flow.

On the other hand, the Monte Carlo method can simulate the change of the angular distribution of the molecular flux both by the collision between molecules and by the change of the nozzle shape, but the same calculation should be repeated whenever the shape of the nozzle changes, as the angular distribution acquired by these methods is not an "analytical solution" but a "numerical solution".

In this paper, an analytical model of the accurate angular distribution of the emitted molecular flux determined via the last intermolecular collisions model and the numerical integration is proposed to express the change of a density of molecules as well as the change of a nozzle shape in the case of a cylindrical nozzle, which is the most commonly used type. Moreover, the model can be helpful to make the optimization processes of nozzle array of linear sources faster and more accurate. The model is verified through a comparison involving the direct simulation Monte Carlo (DSMC) method and an experiment.

Keyword : Linear thermal evaporation system, Intermolecular collisions, Angular distribution, Transitional flow, DSMC
Student Number : 2010-20653

Abstract (Korean)

반도체, OLED의 제조 공정에 주로 사용되는 선형 열 증발원 (Linear Thermal Evaporation System) 방식의 공정은 물질을 담는 도가니와 기화한 물질의 출구 역할을 하는 노즐로 이루어진 장치를 가열하여, 물질을 기화 또는 승화시켜 기판에 박막을 형성하는 방식이다. 기화 또는 승화한 물질의 분자가 노즐을 통과하여 기판에 증착될 때, 기판에 증착된 물질의 두께는 노즐을 통과하여 방출되는 분자 유동의 방사특성 (The angular distribution)에 의해 결정된다. 방사특성은 노즐의 형상, 물질 종류 그리고 밀도에 의해 결정되는데, 이러한 노즐로부터 방출된 분자 유동의 방사특성은 기판에 균일한 두께의 박막을 증착하기 위한 선형 열 증발원을 최적화하는데 있어 중요한 요소 중 하나이다.

이러한 분자 유동의 방사특성을 모델링하기 위해 많은 연구가 진행되었으며, 1907년, 누센(Knudsen)은 원통형 노즐에서 방출되는 분자는 코사인의 지수 함수의 형태(cosnθ)로 나타낼 수 있다는 코사인 법칙(Cosine Law)을 제안하였다. 그러나 누센의 코사인 법칙은 실제 원통형 노즐의 방사특성을 정확하게 표현하기는 한계가 있다.

최근 더 정확하게 분자 유동의 방사 특성을 표현하기 위한 모델로는 수치적분법을 이용하여 노즐에 입사되는 분자의 분포와 노즐의 벽면에서 반사되는 분자의 분포 전체를 적분한 해석적 모델 방법과 몬테카를로 방법을 통해 노즐 출구에서 방출되는 분자의 형태를 시뮬레이션하는 방법이 있다. 이러한 기존 방법들은 노즐의 방사특성을 정확하게 모델링하는데, 큰 기여를 하였다. 하지만 수치적분법을 이용한 방법은 노즐 형상 변화에 의한 방사특성의 해석적 모델을 제안하고 있으나, 분자의 충돌이 없는 경우를 가정하기 때문에 분자의 충돌로 인한 방사 특성의 변화를 나타내지 못한다. 반면, 몬테카를로 방법을 이용한 방법은 분자의 운동 직접적으로 시뮬레이션하기 때문에 분자의 충돌, 그리고 노즐 형태의 변화에 따른 방사 특성의 변화를 나타낼 수는 있으나, 각 변화에 따라 시뮬레이션을 반복해야하는 단점이 있다. 본 연구에서는 일반적으로 많이 사용되는 노즐의 형태인 원통형

노즐에 대해 노즐 내 분자 충돌을 모델을 모델링하고, 수치적분법을 이용, 노즐의 방사특성을 정확하게 나타낼 수 있는 해석적 모델(analytical model)을 제안하고, 모델의 방사특성을 실제 실험과 몬테카를로 시뮬레이션 방법의 방사특성 결과와 비교 검증 하였다.

Keyword : 선형열증발원, 분자간 충돌, 방사특성, 분자 천이 유동, 몬테카를로 시뮬레이션
Student Number : 2010-20653

Table of Contents

Table of Figures

Chapter 1. Introduction

1.1. Study Background

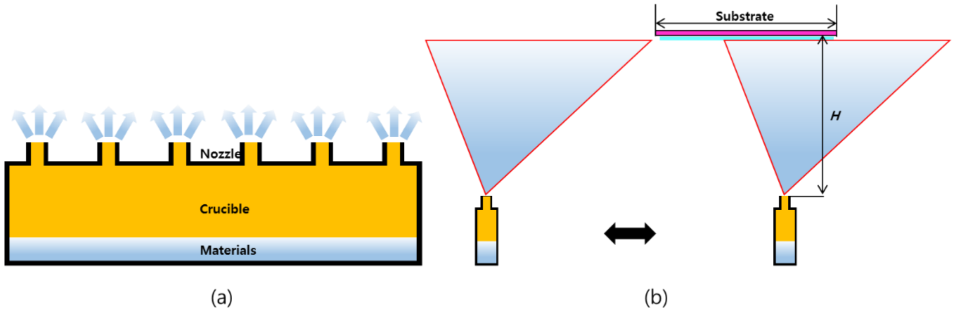

Fig. 1−1. The structure of the linear thermal evaporation source.
(a) The structure of the linear evaporation source. (b) The method of deposition of the linear evaporation system.

In the thin film process required for manufacturing semi-conductors, solar cells and OLEDs, the thermal evaporation system in a high vacuum environment is mainly used to form a thin film of a pure material. In recent years, the linear thermal evaporation system(LS) have been widely used in OLED manufacturing processes, due to the uniform deposition on a wider substrate, the efficiency of materials, and the precise control of positions between a wider substrate and a more precise patterned mask. LS is a method of forming a thin film on a stationary substrate by linearly reciprocating a source having several nozzles, which are generally linearly arranged as shown in Fig. 1. [1]

The optimization of LS is necessary to uniformly deposit material throughout the substrate. In the case of the optimization of LS, the optimization by simulation is better than the optimization by real experimentation. The reason is that LS is processed in a high vacuum environment in order to form a thin film of pure material, when depositing material on the substrate by using LS It takes a long time to make the pressure in the chamber, in which the LS is operated a high vacuum state. Thus the time of heating the LS also takes a long time to reach the temperature at which the material can vaporize or sublimate.

The elements that need optimization include the gap from the linear evaporation source to the substrate, the length between nozzles at both ends, the arrangement, size and slope of the nozzles, and the angular distribution of the molecular flux emitted from the nozzle. In order to optimize each element of the linear evaporation source, the angular distribution of the molecular flux from the nozzle of LS must be known accurately [2] [3].

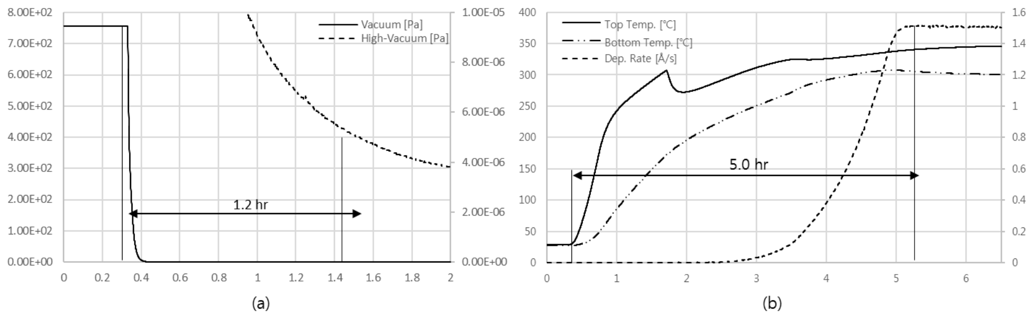

Fig. 1−2. Time required for LS process.
(a) Time to reach high−vacuum (5.0E−06 Pa) (b) Time to reach target rate

1.2. Purpose of Research

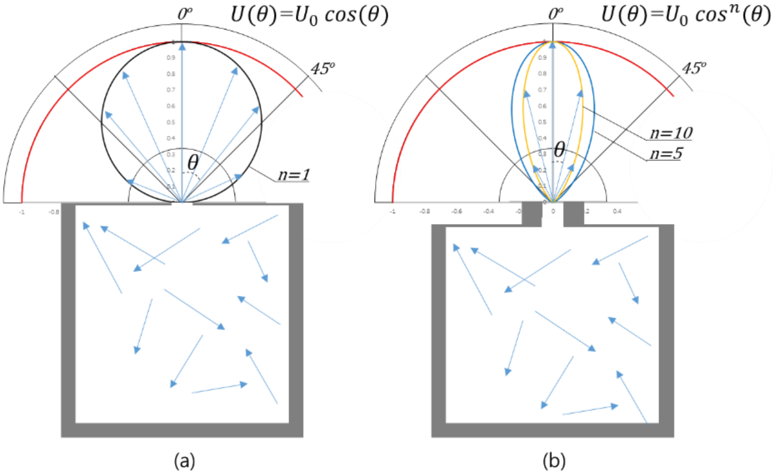

Fig. 1−3. The angular distribution of the molecular flux by Knudsen's Law.
(a) A thin orifice. (b) A long cylindrical nozzle.

The elements influencing the angular distribution of the molecular flux through the nozzle include the type of molecule, the density of molecular flux, and the shape of the nozzle. Many methods by which to gain an accurate calculation of the angular distribution have been devised thus far.

A common and well-known theory is Knudsen's Cosine Law, which is expressed as the n-squared form of the cosine. According to this theory, the angular distribution of the molecular flux emitted from a thin orifice can be expressed in the form of $cos(\theta)$. Additionally, for a relatively long cylindrical nozzle, the angular distribution can be determined in the form of $cos^n(\theta)$, as shown as Fig. 3. [4] [5]

For a cylindrical nozzle, the radius of the outlet and the length of the nozzle affect the changes of the angular distribution of the emitted molecular flux. There is limit to applying the method by Knudsen to LS that needs to optimize the position and size of several nozzles. To overcome the limitation, a model is needed to describe the angular distribution, including the density of the molecular flux and the shape of the nozzle.

A typical method is the analytical model by numerical integration. The molecules entering the nozzle inlet are largely discharged through two paths to the nozzle outlet. The molecules can be divided into molecules that are directly emitted from the nozzle inlet to the nozzle outlet without colliding with the inner wall of the nozzle and molecules emitted to the nozzle outlet after colliding with the inner wall of the nozzle. At this time, the collision with the inner wall can occur once or more than once. The numerical integration method provides a means of calculating the angular distribution of the molecules emitted to the nozzle outlet by multiplying the probability of moving to each path for every molecule entering the nozzle inlet [4].

The analytical model by numerical integration can be applied only to the free molecular flow regime as shown above assumption. Because it is necessary to calculate the probability of the movement path of the nozzle according to the geometrical shape of the nozzle, it can be calculated with a cylindrical nozzle having a relatively simple shape, but it is difficult to calculate this when the shape of the nozzle becomes complicated.

Another method is to use Direct Simulation Monte Carlo (DSMC). DSMC directly tracks the path of a molecule generated by a function having a shape similar to that of the actual angular distribution of the molecular flux entering the nozzle inlet. [6] [7] [8] A part of the molecules is directly emitted toward the nozzle outlet. The other part of the molecules collide with the nozzle wall. Then, the molecules can return to the nozzle inlet, or to the nozzle outlet, or collide with the nozzle wall again. In DSMC, the complicated path of the molecules is not directly calculated, but only change of the direction of the molecules is calculated when there is a collision with the nozzle wall or other molecules. As repeating these calculations, the angular distribution of the molecular flux would be obtained. This is why the angular distribution of the molecular flux emitted from the nozzle by

DSMC can easily be obtained even if the shape of the nozzle or the density of molecules is changed. This DSMC can be utilized to determine accurately the angular distribution of the molecular flux emitted from the nozzle. However, because it is expressed in the form of a numerical solution, the same calculation process must be repeated when the parameters such as the shape of the nozzle and the density of molecules change. Therefore, when using various sizes and arrangements of nozzles, such as a linear source, a considerable amount of time is required for optimization.

In this paper, an analytical solution which overcomes these drawbacks is proposed. It solves the angular distribution of the molecular flux emitted from the nozzle through a modeling of longitudinal density of molecules in transition flow regime. A mathematical model for the angular distribution of the emitted molecular flux from a commonly used cylindrical nozzle was formulated and compared with an existing model. In order to verify the validity of the angular distribution obtained by the model proposed in this paper, the angular distribution obtained through DSMC is used for comparison. In addition, an actual experiment involving the deposition of $Alq3$ using a nozzle of a linear source is conducted.

1.3. Contents of Research

In this study, the analytical model is developed to express exactly the angular distribution of commonly used cylindrical nozzles and compared with existing methods. To achieve this goal, the density of molecules in the regime in which the intermolecular collisions are exist is suggested. The density in the nozzle consists of the existing longitudinal density model of the molecules in free molecular flow by Clausing's equation and a new longitudinal density model of last intermolecular collisions before emitted toward the nozzle outlet. [9] [10]

In the case of the molecules in free molecular flow, some molecules are emitted toward the nozzle outlet without intermolecular collision, the others collide each other in the nozzle before emitted toward the nozzle outlet. In this study, the molecules colliding each other are modeled where in the nozzle last intermolecular collisions are occurred.

Generally, the main issue is to form a pure thin film on a substrate by vaporizing one pure material in linear thermal evaporation system, thus collisions between molecules can be regarded as hard spheres without intermolecular interaction.

When the molecules collide with the inner wall of the nozzle or other molecule, the direction of the reflected molecule follows Knudsen's cosine law($U(\theta) = cos(\theta)$). That is, the molecules that collide with the inner wall of the nozzle can be reflected in all directions regardless of the direction of incidence. This assumption makes it possible to take into account only how many molecules are at a position in the nozzle, without the need to consider the motion of the molecules before collision, when determining the direction of the molecules after colliding with an inner wall of the nozzle or other molecules.

In order to verify the angular distribution of the molecular flux emitted from the nozzle calculated in this way, the real experiment depositing materials on a substrate and DSMC are used. And the angular distribution by the real experiment and by DSMC are compared with the angular distribution by this study.

Since the new analytical model suggested by this study is a function including the design of the nozzle (the radius and length of the nozzle) and the density of the molecules (mean free pass, MFP) as variables, it is possible to predict how the angular distribution will change as the design of the nozzle and the density of the molecules change.

Chapter 2. Background Theory

2.1. The Calculation of Thickness of Molecules Deposited on a Substrate

2.1.1. The amount of the molecules deposited on unit area of the substrate with a single nozzle

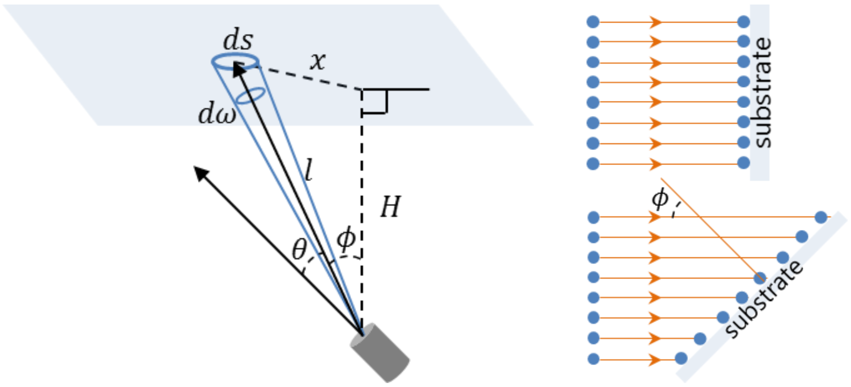

Fig. 2−1. The molecules deposited on unit area of the substrate with a single nozzle

The thickness of the molecules emitted throughout the nozzle on the substrate can be represented by the relationship between the position of the substrate and the nozzle center. The number or thickness of the molecules deposited at height H and a distance x apart from the nozzle is as follows.

$$m = U(\theta)\frac{d\omega}{ds} \quad (2.1)$$

Where $U(\theta)$ is the angular distribution of the molecular flux emitted from the nozzle, $d\omega$ is the solid angle and ds is the unit area of the substrate. The unit area ds can be express as follows, when the angle between the nozzle and the substrate is ϕ. The thickness of the molecules deposited on the unit area of the substrate can be re-described as Eq. (2.3).

$$ds = \frac{l^2 d\omega}{cos(\phi)} \quad (2.2)$$

$$m = U(\theta)\frac{cos(\phi)}{l^2} = U(\theta)\frac{cos(\phi)}{x^2+H^2} \quad (2.3)$$

2.1.2. The amount of the molecules deposited on a substrate with LS

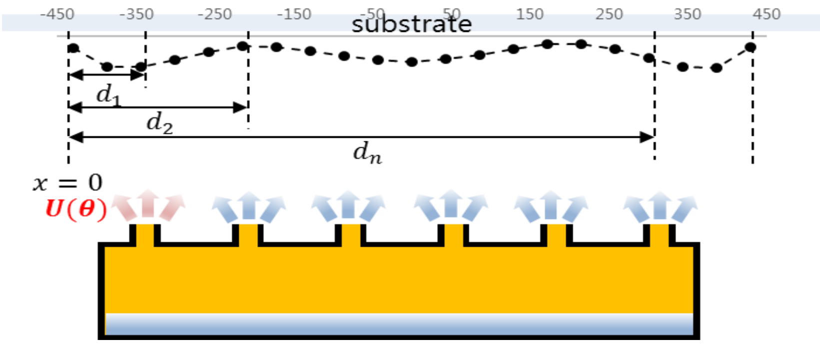

Fig. 2-2. The thickness profile from LS with n-nozzles

The thickness of molecules deposited on the substrate for a single nozzle has been mentioned in the previous discussion. When $m(x)$ is the thickness profile of cross-section of the molecules deposited on the substrate from a single nozzle with the angular distribution $U(\theta)$, The thickness profile from LS with n-nozzles can be calculated. The total thickness of the molecules from LS is calculated by adding the thickness profile of all nozzles up, when d_n, c_n mean the position and the conductance of the nth nozzle, respectively.

$$m_{total} = \sum c_n m(x - d_n) \tag{2.4}$$

$$c_{1,2\ldots n} : Conductance\ of\ n^{th}\ nozzle \tag{2.5}$$

$$d_{1,2\ldots n} : Position\ of\ n^{th}\ nozzle \tag{2.6}$$

At this time, the uniformity of the molecules is shown on the substrate in a uniform manner. Uniformity can be expressed as the thickness of the thickest part m_{max}, and the thickness of the thinnest part m_{min}.

$$uniformity\ [\%] = \frac{m_{max}(x) - m_{min}(x)}{m_{max}(x) + m_{min}(x)} \times 100 \tag{2.7}$$

$$m_{max} : The\ thickest\ thickness\ in\ the\ substrate$$

$$m_{min} : The\ thinnest\ thickness\ in\ the\ substrate$$

2.2. The Angular Distribution by Knudsen

2.2.1. Knudsen's cosine law

Knudsen introduced the kinetic molecular dynamics through a study of rarefied gases passing through a tube in 1907. When a molecule incident on a wall is reflected after colliding against a wall surface, it has the same probability in all directions regardless of the incident direction of the molecules. When the angle between the direction in which molecules are reflected and the direction perpendicular to the wall is θ, the angular distribution of the reflected molecules could be expressed as $cos(\theta)$.

In the case of a molecular flow emitted from a very thin orifice, its angular distribution could be defined as a same angular distribution from plane with the same area as the orifice. [11] [12]

In the case of a nozzle with a long length, the angular distribution of the molecular flux from the nozzle is similar to the shape of $cos^n(\theta)$. Because the density in the vertical direction increase by beaming effect of the molecules. [13]

$$du = \frac{d\omega}{\pi} cos(\theta)$$

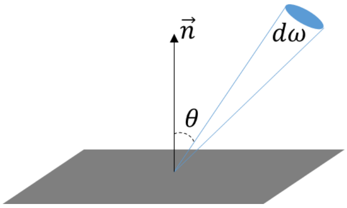

Fig. 2−3. The probability of emission at angle θ relative to surface normal

2.2.2. The problem of Knudsen's cosine law

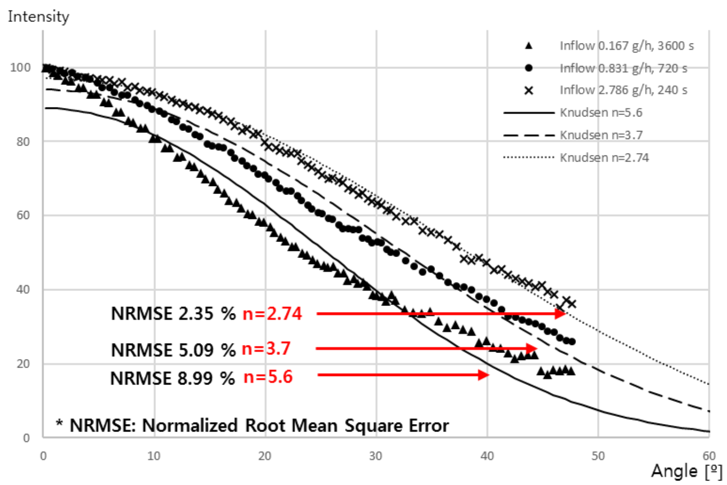

Fig. 2−4. The comparison of the angular distribution by Knudsen and experiment

The analytical model of the angular distribution of the molecular flux by using the cosine function proposed by Knudsen contributed greatly to the theory of thin film deposition.

However, Knudsen 's theory had a limitations to applied to the optimization of LS with several various nozzles, used to forms a uniform thin film on a wide area substrate. Since various types of angular distribution can be expressed by Knudsen 's theory as $cos^n(\theta)$, it can express the change of the angular distribution by change of the molecular inflow as well as change of the design of the nozzle. In order to find the optimized n value, However, it was necessary to find the angular distribution through the actual experiment and fit the n value.

Furthermore, there is a limit to accurately fitting all ranges of angular distribution. Fig. 2−4 is a graph showing a comparison between the angular distribution obtained by the results of the actual experiment when the molecular inflow into a single nozzle of LS is changed and the angular distribution fitted by Knudsen's law with the optimized n value.

It is well matched with Knudsen's law when the molecular inflow was $2.786 g/h$, but the error increased as the molecular inflow decreased. Using the normalized root mean square error(NRMSE), which can be used to quantify the error between the angular distribution by two methods, the NRMSE is 2.35%, 5.09%, and 8.99% when n is 2.74, 3.70, and 5.60 for each molecular inflow, respectively.

$$NRMSE[\%] = \sqrt{\frac{\sum_{\theta=0}^{n}\left(U_1(\theta)-U_2(\theta)\right)^2}{n}} \Big/ \overline{U_2}(\theta) \tag{2.8}$$

NRMSE can be obtained by dividing the square root of the average of the error squared of each component value by the average of the comparison values.

2.3. The Angular Distribution by the Numerical Integration

2.3.1. The calculation of the numerical integration

There are two paths that the molecules entering the nozzle inlet are mainly discharged to the nozzle outlet. One is directly emitting from the nozzle inlet to the nozzle outlet without colliding with the inner wall of the nozzle and the other is emitting to the nozzle outlet after colliding with the inner wall of the nozzle. The numerical integration method provides a means of calculating the angular distribution of the molecules emitted to the nozzle outlet by multiplying the probability of moving to each path for every molecule entering the nozzle inlet. Because it is necessary to calculate the probability of the movement path of the nozzle according to the geometrical shape of the nozzle, it can be calculated with a cylindrical nozzle having a relatively simple shape, but it is difficult to calculate this when the shape of the nozzle becomes complicated. For the method, several assumptions as follows are necessary. [14]

- The flow is a free molecular flow; i.e. the molecules do not collide with each other.

- The flow is steady; i.e. the inflow of the molecules keep constant.

- At the nozzle inlet, molecules enter the nozzle inlet evenly in position and coincide with the cosine law in terms of the angle.

- At the nozzle outlet, molecules are emitted at the center.

- The inflow of the molecules equals the reflectance rate of the molecules at any point on the inner wall of the nozzle.

- After colliding with the inner wall of the nozzle, molecules still follow the cosine law when reflecting.

- The molecules emitted from the nozzle are not taken into account again; i.e. the backflow from the outlet is neglected.

2.3.2. The molecules directly emitted toward the nozzle outlet from the nozzle inlet

The molecules directly emitted from the unit area of the nozzle inlet dS to outlet area element dA are shown in Fig.7. L and R are the nozzle length and radius respectively. $\vec{r_i}$ is the radius vector from the center of the nozzle inlet to dS. $\vec{r_o}$ is the radius vector from the center of the nozzle outlet to dA . θ_1 is the angle between $\overline{OA}$ and $\overline{OB}$. ϕ is the angle between $\overline{AB}$ and $x-axis$, and it is defined as "azimuth an1gle". d is the diameter of the nozzle, $d=2R$. ρ_1 is the vector from dS to dA. β is the angle between vector ρ_1 and normal line of dA , and it is defined as "polar distance angle". ρ_1 could be obtained as follows.

$$\rho_1^2 = L^2 + \overline{AB}^2 \quad (2.10)$$

ρ_1 in Eq. (2.12) is calculated by merging Eq. (2.10) with $\overline{AB}^2 = r_i^2 + r_o^2 - 2r_i r_o\, cos(\theta_1)$.

$$\rho_1^2 = L^2 + r_i^2 + r_o^2 - 2r_i r_o\, cos(\theta_1) \quad (2.11)$$

According to the cosine law, the number of molecules directly emitted from the unit are of the nozzle inlet dS to the unit are of the nozzle outlet dA is given by

$$dN_{dS-dA}(r_o) = \gamma dS \frac{1}{\pi} cos^2(\beta) \frac{1}{\rho_1^2} dA \quad (2.12)$$

Where γ is the molecular inflow at the nozzle inlet. $dS = r_i dr_i d\theta_1$ could be substituted into Eq. (2.12). Eq. (2.12) could be re-scribed as

$$dN_{dS-dA}(r_o) = \gamma \frac{1}{\pi} \frac{L^2}{\rho_1^4} r_i dr_i d\theta_1 dA \quad (2.14)$$

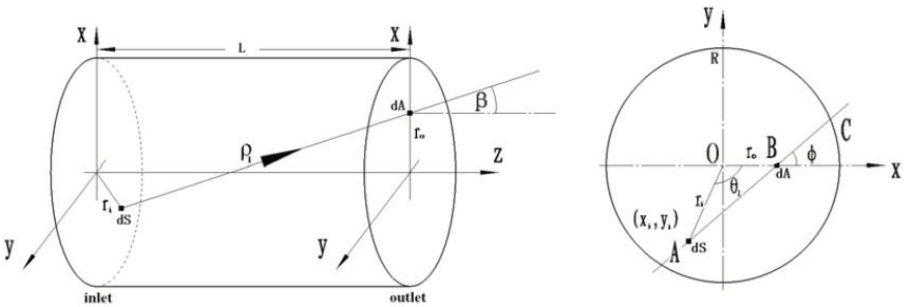

Fig. 2−5. The model for directly emitted molecules from the nozzle inlet to the nozzle outlet.

By integrating dr_i and $d\theta_1$, the number of molecules directly emitted from whole nozzle inlet cross section to dA could be acquired.

$$dN_{S-dA}(r_o) = \frac{\gamma L^2}{\pi} dA \int_0^R dr_i \int_0^{2\pi} \frac{r_i}{\rho_1^4} d\theta_1 \qquad (2.15)$$

2.3.3. The molecules emitted toward the nozzle outlet after colliding with the inner wall of the nozzle

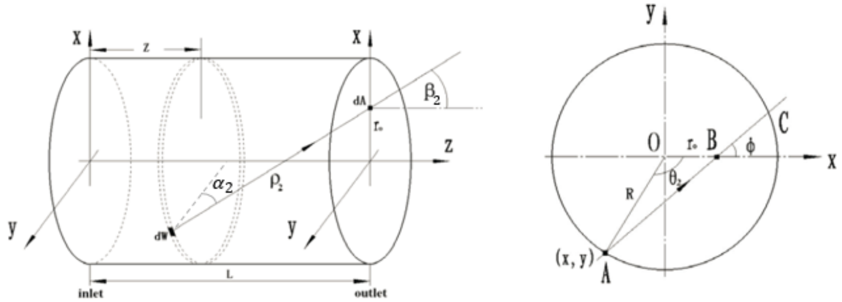

Fig. 2−6. The model for reflective molecules from nozzle wall to nozzle outlet

The molecules emitted toward the unit are of the nozzle outlet dA after colliding with the unit are of the inner wall dW are shown in Fig. 8. z is the axial distance from the nozzle inlet to dW. θ_2 is the angle between $\overline{OA}$ and $\overline{OB}$. β_2 and ϕ are the "polar distance angle" and "azimuth angle" respectively. α_2 is the angle between ρ_2 and the normal line of dW ρ_2 is the vector from dW to dA. ρ_2 could be expressed as

$$\rho_2^2 = (L - z)^2 + R^2 + r_o^2 - 2Rr_o\, cos(\theta_2) \qquad (2.16)$$

β_2 and α_2 are given by $cos(\beta_2) = (L - z)/\rho_2$ and $\cos(\alpha_2) = \sqrt{R^2 + r_o^2 - 2Rr_o\, cos(\theta_2)}/\rho_2$ respectively. According to the cosine law, the number of molecules emitted from the unit are of the inner wall dW to dA at the nozzle outlet after a collision with the inner wall of the nozzle is given by

$$dN_{dW-dA}(z, r_o) = \gamma_2(z) dW \frac{1}{\pi} cos(\alpha_2)\, cos(\beta_2) \frac{1}{\rho_2^2} dA \qquad (2.14)$$

Where $\gamma_2(z)$ is the molecule reflectivity at dW. As $\gamma_2(z) = Rd\theta_2 dz$, the total number of molecules emitted from whole inner wall of the nozzle to dA at the nozzle outlet is

$$dN_{W-dA}(r_o) = \frac{R}{\pi} dA \int_0^L \gamma_2(z) dz \int_0^{2\pi} \frac{\sqrt{R^2 + r_o^2 - 2Rr_o cos\theta_2}(L - z)}{\rho_2^4}\, d\theta_2 \quad (2.19)$$

2.3.4. The analytical model of the numerical integration

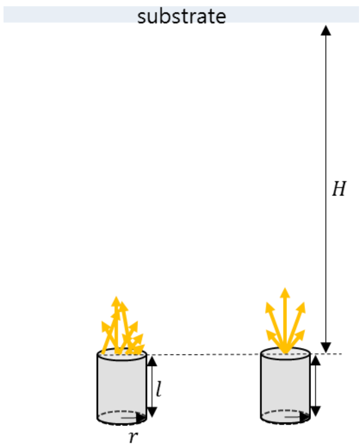

Fig. 2−7. The approximation for the analytical model of numerical integration

In the previous content for numerical integration, the numerical method calculating the number of molecules emitted to the unit area of the nozzle outlet dA was discussed. Numerical integration was not the analytical method but the numerical method because it uses a numerical method to calculate all the paths of the molecules emitted to all the positions of the nozzle inlet and all positions of inner wall of the nozzle toward all positions of the nozzle outlet.

The molecules emitted from the nozzle actually are discharged evenly in position at the nozzle outlet as shown in Fig. 9. It is approximated that all the molecules are emitted from the center of the nozzle outlet to represent the analytical method.

Generally, the gap distance between LS and the substrate is at least several tens to several hundreds longer than the nozzle radius in a typical thermal evaporation system. Therefore, there is little error, even if the approximation assuming the molecules are emitted from the center of the nozzle outlet.

The analytical model of the angular distribution for a cylindrical nozzle with the length l, and the radius r is as follows in Eq. (2.23) and Eq. (2.24). The analytical model of the angular distribution is divided into two models based on $tan(\theta_{cr}) = 2r/l$. With this model, θ_{cr} is referred to as the critical angle. The density of the molecules $\rho(z)$ in the nozzle is as follows:

$$\rho(z) = az + b = \frac{(1-2\xi_0)}{l} z + \xi_0 \tag{2.20}$$

The density of molecules at the nozzle outlet $(z = 0)$ is determined as follows:

$$\xi_0 = \frac{1+\gamma^2-\sqrt{1+\gamma^2}}{\gamma\sqrt{1+\gamma^2}+\gamma^2} \tag{2.21}$$

The density of molecules at the nozzle inlet $(z = l)$ is determined using the equation below.

$$\xi_1 = 1 - \xi_0 \tag{2.22}$$

Here, γ refers to the aspect ratio of the diameter to the length of the nozzle $\gamma = 2r/l$. When $tan(\theta)$ is larger than the aspect ratio of the nozzle, the only reflected molecules emitted after a collision with nozzle wall could be emitted toward the nozzle outlet.

- $tan(\theta) > 2r/l$

$$U(\theta) = 4r^2 \cos(\theta) \left(\frac{a}{3} \frac{2r}{tan(\theta)} + \frac{b\pi}{4} \right) \tag{2.23}$$

Both molecules directly emitted without collisions and reflected molecules emitted after a collision with the nozzle wall could exist. In this case, the value of $tan(\theta)$ of the emitted molecules is smaller than the aspect ratio of the nozzle.

- $tan(\theta) < 2r/l$

$$U(\theta) = 4r^2 \cos(\theta) \left[a \frac{2r}{tan(\theta)} \left(\frac{1-\sin^3(\varphi_l)}{3} \right) + b \left(\frac{\pi}{4} - \frac{1}{2}\varphi_l + \frac{1}{2}\sin(\varphi_l)\cos(\varphi_l) \right) \right]$$
$$+2c * \cos(\theta) \left(r^2 \varphi_l - \frac{r\,l}{2} tan(\theta) \sin(\varphi_l) \right) \tag{2.24}$$

$$\varphi_l = \cos^{-1}\left(\frac{l\,tan(\theta)}{2r} \right) \tag{2.25}$$

c of Eq. (2.24), i.e., the density of the molecules on the inner wall of the nozzle inlet, would be $c = 1$, Because a and b of Eq. (2.23) and Eq. (2.24) are normalized values by Clausing's equation. [15]

2.3.5. The problem of the numerical integration

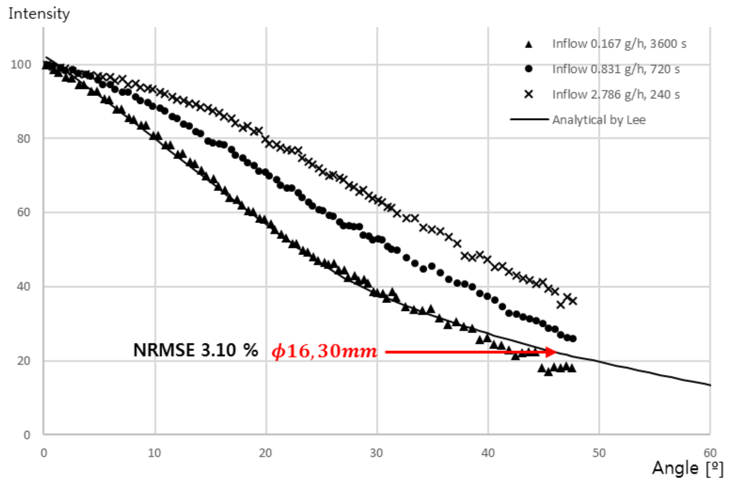

Fig. 2-8. The comparison of the angular distribution by the numerical integration and experiment

The numerical integration of the angular distribution of the molecular flux through the nozzle using the information of the design of the nozzle makes it possible to predict the angular distribution unlike Knudsen 's law which requires the pre-examination for the fitting. As shown in Fig. 2-8, NRMSE is consistent with 3.10% when compared with the angular distribution of the molecular flux through the actual nozzle.

In the case of the numerical integration, however, Since the molecular flux through the nozzle is assumed to be a free molecular flow in which collisions between molecules are negligible, the angular distribution can not be predicted when collisions between molecules exist such as the high molecular inflow.

2.4. Direct Simulation Monte Carlo (DSMC)

2.4.1. The Calculation of DSMC

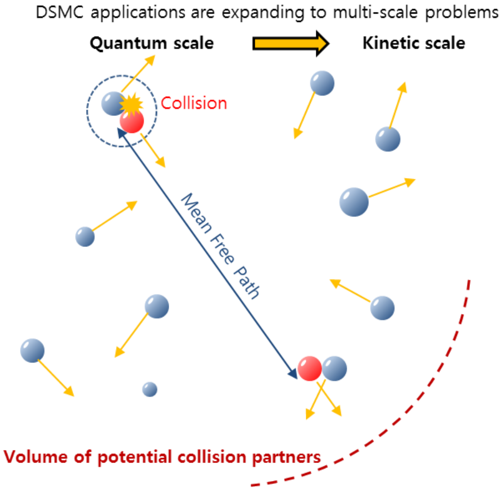

Fig. 2-9. DSMC applications are expanding to multi-scale problems

Monte Carlo simulation is a multi-scale algorithm that allows Molecular Dynamics (MD) on the Quantum scale to be interpreted on a larger hydrodynamic scale such as kinetic scale. In general, when MD is expanded to hydrodynamic scale, the amount of information is so large that the calculation becomes complicated and difficult. DSMC is the function stochastically calculating variables such as the motion or the collision of molecules. A deterministic model that can accurately compute the outcome of a given variable is generally an analytical solutions. However, a probability model that can not accurately predict the outcome is generally impossible to find analytical solutions. In this case, the solution must be found by a numerical method. DSMC is the method [16]

Direct Simulation Monte Carlo(DSMC) is the dominant numerical method at the kinetic scale. MD is inefficient for simulating the kinetic scale because computational time step of MD is limited by time of collision. It is so short that MD is inefficient in the kinetic scale. On the other hand, the relevant time scale of DSMC is mean free time. Therefore, the time step of DSMC is large because collisions are evaluated stochastically.

Since the development of DSMC by Graeme Bird in the late 1960s, research has been actively conducted and has been applied and developed in the following fields.

- DSMC developed by Graeme Bird (late 60's)
- Popular in aerospace (70's)
- Variants & improvements (early 80's)
- Applications in physics & chemistry (late 80's)
- Used for micro/nano-scale flows (early 90's)
- Extended to dense gases & liquids (late 90's)
- Used for granular gas simulations (early 00's)
- Multi-scale modeling of complex fluids (late 00's) [7] [8]

2.4.2. The problem of DSMC

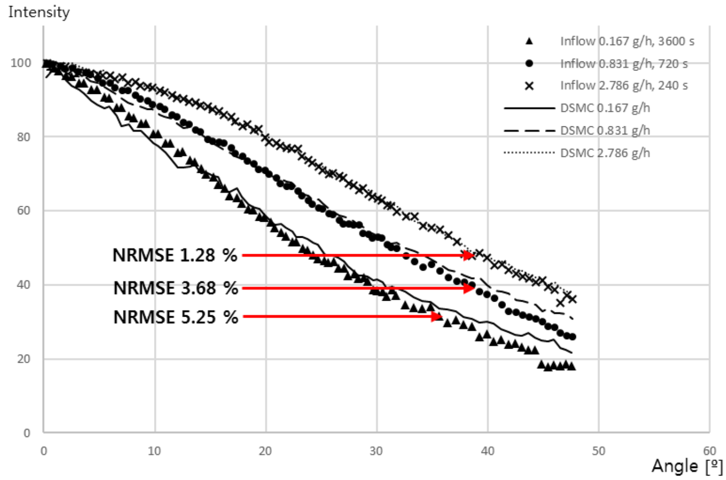

Fig. 2-10. The comparison of the angular distribution by DSMC and experiment

DSMC is a typical numerical model that stochastically simulates the molecular dynamics by including both the design of the region, in which the molecule exists, and the type and density of the molecule. Therefore, the angular distribution simulated by DSMC be matched almost accurately with the actual angular distribution. The results show that the NRMSE are 1.28%, 2.68%, and 5.25%, respectively, when compared with the experimental results.

Thus, DSMC is a theory that not only predicts the angular distribution by influence of the design of the nozzle, but also by influence of the type of density of the molecules. However, even if the calculation is performed stochastically for the fast simulation on the kinetic scale, the simulation time is still several hours longer than the analytical model, which can predict the angular distribution in a few seconds.

Chapter 3. Modeling of the Angular Distribution of Molecular Flux from Cylindrical Nozzle

3.1. Assumptions for Modeling

In this paper, the angular distribution of the molecular flow from the nozzle by the density of the molecules in the nozzle as well as the design of the nozzle is calculated. To do this, the paths emitting the molecules are largely divided into the path of the emission directly to the nozzle outlet at the nozzle inlet and the emission to the nozzle outlet after colliding with the inner wall of the nozzle, similarly to the analytical model using the numerical integration described above. However, unlike the conventional analytical model, there are molecular collisions that are not in the free molecular flow. Therefore, the following new assumptions are additionally needed with part of the assumptions of the conventional analytical model. [14]

- The flow is steady; i.e. the molecular inflow keep constant.
- At the nozzle inlet, molecules enter the nozzle evenly in position and coincide with the cosine law.
- At the nozzle outlet, molecules are emitted at the center.
- The rate of molecular inflow equal the rate of reflectance at any point on the inner wall of the nozzle.
- After colliding with the inner wall of the nozzle, molecules still follow the cosine law.
- The molecules emitted from the nozzle are not taken into account again; i.e. the backflow from the outlet is neglected.

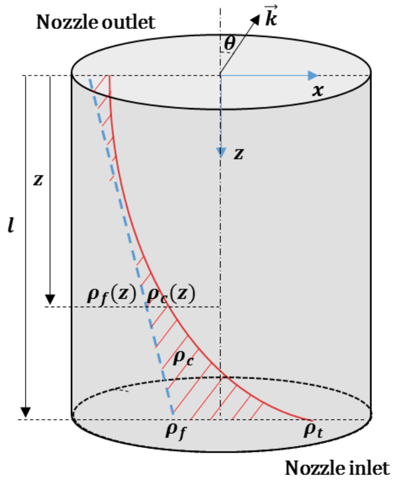

Fig. 3−1. Total density consist of density of free molecular flow and density of intermolecular collisions

- The flow includes a transitional flow regime; i.e. the molecular collisions exist.

- The total molecular density ($\rho_t(z)$) in nozzle consists of the density of free molecular flow ($\rho_f(z)$) by Clausing's equation and the density of intermolecular collisions ($\rho_c(z)$) as shown in Fig. 11.

- The density of intermolecular collisions ($\rho_c(z)$) is for the last collision before emitted to the nozzle outlet. Therefore, there is no more collision.

- The chemical reaction can be negligible. The conservation of energy and linear momentum can be satisfied. [17]

- The number of the molecules emitted toward the nozzle outlet in free molecular flow depends on the probability of free travelling distance ($p(t, \lambda_m)$). [18] [19]

The above assumptions are satisfied, and the molecules emitted from the nozzle in the new model can be divided into four cases as shown in Fig 12.

The CASE I. and CASE II. are for free molecular flow. In the first case, molecules of free molecular flow are emitted toward the nozzle outlet after collision with the inner wall of the nozzle.

The CASE II. is the case where it is directly emitted from the nozzle inlet toward the nozzle outlet. In both cases, the molecules depend the probability of a molecule travelling to the nozzle outlet without any collision.

In the CASE III. and CASE IV., intermolecular collisions exist. The CASE III. is that the molecules that collide with the other molecules re-collide with an inner wall of the nozzle and then go to the nozzle outlet. The CASE IV. is after a collision between molecules occurs and then the molecules are directly emitted toward the nozzle outlet. In the CASE IV, the density of the last intermolecular collisions is evenly distributed in the cross-section. In these two cases, the density is a function about the last collision between the molecules, so it is emitted to the nozzle outlet at a 100 percent probability without any other collision.

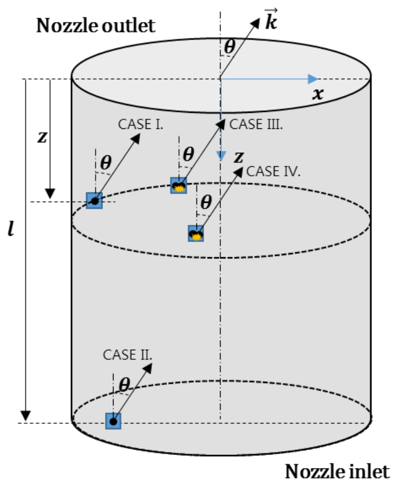

Fig. 3-2. The four cases of the molecules that can be emitted toward the nozzle outlet

3.2. Modeling of the Longitudinal Density in a Cylindrical Nozzle

In this paper, the analytical model is mainly two types of the molecules. One is the molecules passing through the nozzle outlet without any intermolecular collision and the other is the molecules passing through the nozzle outlet after colliding with other molecules. Knudsen defined whether there is an intermolecular collision inside the nozzle or not, and the kind of molecular flow was classified according to the frequency of collision. [20] The Mean Free Path (MFP) λ_m is defined as follows:

$$\lambda_m = \frac{1}{\sqrt{2}\pi d^2 n_v} \tag{3.1}$$

Here, d is the diameter of the molecules, and n_v is the number of the molecules per unit volume. The ratio of the mean free path to the nozzle diameter can be used to describe types of flow. This ratio is referred to as the Knudsen number. The Knudsen number of the molecules with MFP λ_m in the nozzle with the radius r is as shown as Eq. (3.2).

$$K_n = \frac{\lambda_m}{2r} \tag{3.2}$$

The type of flow is characterized by the value of the Knudsen number. Profiles of the various types of flow regimes are shown in Fig. 13. [20] [21]

The regime of the Knudsen flow the Molecular flow can be further subdivided as shown in Fig. 14. For $K_n < 0.001$, called continuum flow regime, in the continuum flow regime, the flow can be analyzed by using the Navier-Stokes equations with conventional no-slip boundary conditions. For $0.001 < K_n < 0.1$, named slip-flow regime, the rarefaction effects begin to influence in the flow.

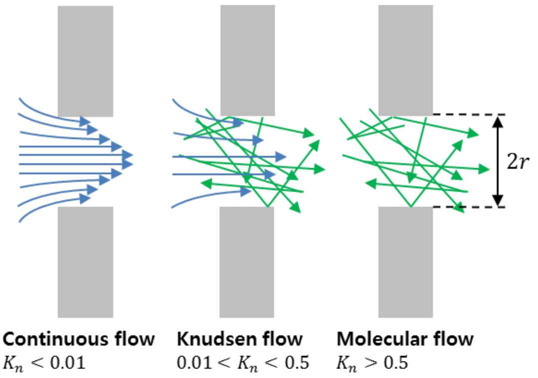

Fig. 3-3. Profiles of the various types of flow regimes

For $10.0 > K_n > 0.1$, the flow is characterized as transitional flow, as the density of molecules becomes more rarefied. For this regime, as the continuum assumption of the Navier-Stokes equations is no longer established, alternative simulation techniques such as DSMC can be adopted. For the $K_n > 10.0$, the regime can be described as a free molecular flow. In this flow, little molecules are collide each other. [22]

$$\begin{array}{ll} K_n > 10.0 & \text{Free Molecular flow} \\ 0.1 < K_n < 10.0 & \text{Transitional flow} \\ 0.001 < K_n < 0.1 & \text{Slip flow} \\ K_n < 0.001 & \text{Contimuum flow} \end{array} \tag{3.3}$$

The conventional analytical model has suggested the angular distribution of the free molecular flow in the nozzle. In this study, the angular distribution of the molecular flow include the transitional flow in which there are intermolecular collision as well as the free molecular flow aim to be modeled.

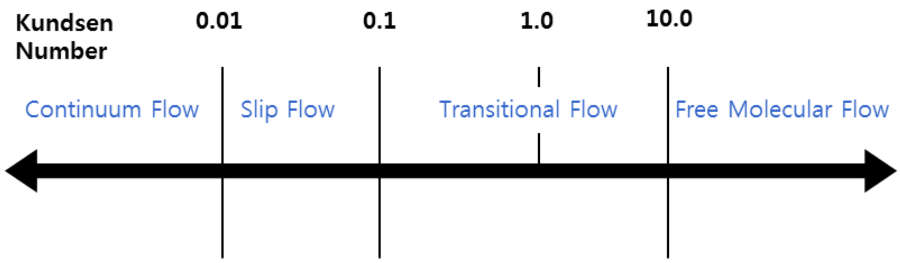

Fig. 3-4. Type of flow regime based on the Kindsen number

To do this, the longitudinal density of the last intermolecular collision before being emitted to the nozzle outlet is modeled as well as the longitudinal density of the existing free molecular flow.

3.2.1. The longitudinal molecular density of free molecular flow

As in conventional analytical model, the longitudinal density of the molecules inside the nozzle follows the Clausing's equation. [9] [19] Assuming the density $\rho_f(z)$ in the nozzle at a distance of z away from the nozzle outlet, varies linearly along the nozzle as shown in Fig. 16, an approximation which has been shown to be quite accurate for free molecular flow.

$$\rho_f(z) = az + b \tag{3.4}$$

Clausing's equation provided a useful check for the numerical integration, although this is derived for the free molecular flow region and does not appear to have been used previously in other regimes. When ξ_0 and ξ_l are the density of the molecules at the nozzle inlet and outlet, respectively, and γ refers to the ratio of the diameter to the length of the nozzle, $\gamma = \frac{2r}{l}$, the density of molecules at the nozzle outlet $(z = 0)$ is determined as follows:

$$\xi_0 = \frac{1+\gamma^2-\sqrt{1+\gamma^2}}{\gamma\sqrt{1+\gamma^2}+\gamma^2} = \rho_f(0) \tag{3.5}$$

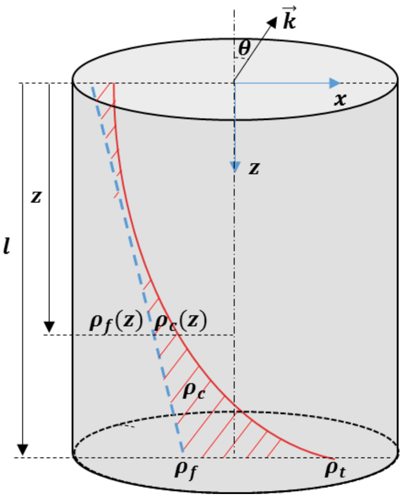

Fig. 3−5. The total density in the nozzle consist of the free molecular density, $\rho_f(z)$ and the intermolecular collision density, $\rho_c(z)$

The density of molecules at the nozzle inlet ($z = l$) is determined using the equation below.

$$\xi_l = 1 - \xi_0 = \rho_f(l) \tag{3.6}$$

3.2.2. The longitudinal density of last intermolecular collisions

In the case of the existence of the intermolecular collisions, even if the molecules inside the nozzle is distributed satisfying the Clausing's equation, the some molecules can not be emitted toward the nozzle outlet by the intermolecular collision. The molecules is not considered the molecules emitted from the initial position by Clausing's equation, but the molecules emitted from the position where the collision occur. Therefore, it is necessary to model the longitudinal density inside the nozzle for the last collision between the molecules before being discharged to the nozzle outlet.

In the free molecular flow, the distribution of molecules inside the nozzle is known as a linear model. Therefore, the last intermolecular collision density inside the nozzle $\rho_c(z)$ is proportional to the n-square of the molecular density, so it can be regarded as linear. Therefore, the collision density model of molecules is as shown as eq. (3.7).

$$\rho_c(z) = (\alpha z + \beta)^n \tag{3.7}$$

The number of the intermolecular collisions M_{col} can be defined as the expression by MFP and the number of the molecules in the nozzle. Since MFP is also inversely proportional to the number of molecules, the number of the intermolecular collisions inside the nozzle M_{col} is proportional to the third power as Eq. (3.6).

$$M_{col} = \frac{1}{2}N(N-1)\frac{\bar{v}\tau}{\lambda_m} \propto N^3 \tag{3.8}$$

Here, N is the number of molecules, $\bar{v}$ is the average velocity of the molecules and τ is the unit time step. The longitudinal density of the last intermolecular density Eq. (3.7) can be re-describe as shown as Eq. (3.9), using Eq. (3.8).

$$\rho_c(z) = (\alpha z + \beta)^3 \qquad (3.9)$$

However, the position of the last intermolecular collision before emission toward the nozzle outlet does not depend solely on the density of the molecules. For example, the probability that a collided molecule near the nozzle inlet will be emitted without another collision until it reaches the nozzle outlet, and the probability that a collided molecule near the nozzle outlet will pass through the nozzle outlet is different. Therefore, the values of α and β should be defined by using the last intermolecular collisions at the nozzle inlet $\rho_c(l)$ and the nozzle outlet $\rho_c(0)$ which are easy to predict.

$$\alpha = \frac{(\rho_c(l))^{\frac{1}{3}} - (\rho_c(0))^{\frac{1}{3}}}{l} \qquad (3.10)$$

$$\beta = \left(\rho_c(0)\right)^{\frac{1}{3}} \qquad (3.11)$$

The number of all intermolecular collisions in the nozzle c_{tot} can be obtained by using the longitudinal molecular density by Clausing's equation.

$$c_{tot} = \left(\frac{\rho_f(l)+\rho_f(0)}{2} l\right)^2 \Big/ 2\lambda_m \qquad (3.12)$$

The intermolecular collisions at the nozzle inlet is proportional to the square of the number of molecules at the nozzle inlet, so it can be expressed as Eq. (3.13).

$$c_l = \frac{\left(\frac{\rho_f(l)+\rho_f(0)}{2} l\right)^2}{2\lambda_m} \rho_f^2(l) \qquad (3.13)$$

The molecules collided with other molecules at the nozzle inlet can reach the nozzle outlet depending the probability of free travelling distance ($p(t, \lambda_m)$). The density of the last intermolecular collisions at the nozzle inlet $\rho_c(l)$ is as follows:

$$\rho_c(l, \lambda_m) = \left(\frac{\rho_f(l)+\rho_f(0)}{2} l\right)^2 \Big/ 2\lambda_m \, \rho_f^2(l)\, exp\left(-\frac{\rho_f(l)+\rho_f(0)}{2} \frac{l}{\lambda_m}\right)$$

$$= \frac{l\,\xi_l^2}{8\lambda_m} exp\left(-\frac{l}{2\lambda_m}\right) \tag{3.14}$$

The density of the last intermolecular collision at the nozzle outlet $\rho_c(0)$ can also be calculated as follows:

$$\rho_c(0, \lambda_m) = \left(\frac{\rho_f(l) + \rho_f(0)}{2} l\right)^2 \Big/ 2\lambda_m \rho_f^2(0) = \frac{l\,\xi_0^2}{8\lambda_m} \tag{3.15}$$

3.3. Modeling of the Molecules without the Inter-molecular Collisions

3.3.1. The molecules emitted toward the nozzle outlet after a collision with the inner wall of the nozzle (CASE I.)

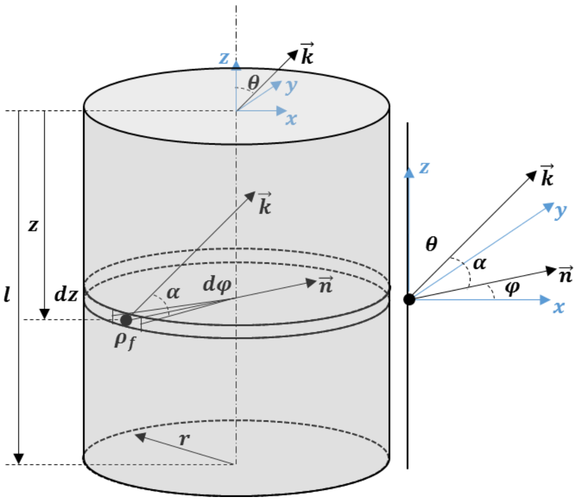

Fig. 3−6. The molecules emitted after colliding with an inner wall of the nozzle in the $\vec{k}$−direction.

The molecules emitted in the $\vec{k}$−direction after colliding with an inner wall of the nozzle are depicted in Fig. 16. The vector $\vec{k}$ serves as a unit vector with the angle between z−axis and the vector $\vec{k}$ is θ and the angle between x−axis and the vector $\vec{k}$ is φ in the spherical coordinate system. When converting into the Cartesian coordinate system,

$$\vec{k} = (1,\ \theta,\ \varphi) = \left(sin(\theta)\,cos(\varphi),\ sin(\theta)\,sin(\varphi),\ cos(\theta)\right) \quad (3.16)$$

The vector $\vec{n}$ serves as a unit vector with the angle between the x−axis and the vector $\vec{n}$ is φ and normal to the inner wall of the nozzle. If the vector $\vec{k}$ is on the $x - z$ plane, $\vec{k}$ and $\vec{n}$ are expressed as follows:

$$\vec{k} = \left(sin(\phi),\ 0,\ cos(\phi)\right) \quad (3.17)$$

$$\vec{n} = \left(cos(\varphi),\, sin(\varphi),\, 0\right) \tag{3.18}$$

When the angle between $\vec{k}$ and $\vec{n}$ is α degrees, the inner product of the two vectors is as follows:

$$\vec{k}\circ\vec{n} = \left|\vec{k}\right||\vec{n}|cos(\alpha) = sin(\theta)cos(\varphi) \tag{3.19}$$

The angle α can be expressed as a function of θ and φ by using Eq. (3.19).

$$cos(\alpha) = sin(\theta)\,cos(\varphi) \tag{3.20}$$

The number of molecules emitted in the $\vec{k}$-direction from a unit area dU_I can be expressed as follows,

$$dU_I(\theta) = \rho_f(z)\cos(\alpha)\,rd\varphi dz, \tag{3.21}$$

where $\rho_f(z)$ is the molecular density of the free molecular flow by Clausing's equation, $cos(\alpha)$ is the number of molecules emitted toward the $\vec{k}$-direction on the inner wall of the nozzle, and $rd\varphi dz$ refers to the unit area of the nozzle. Not the all molecules emitted in the $\vec{k}$-direction on the inner wall of the nozzle can be discharged through the nozzle outlet. Some molecules collide with other molecules inside nozzle and have different vectors. Therefore, the molecules having no collision can be emitted toward the nozzle outlet. The molecules follow the probability of free travelling distance $p(t,\lambda_m)$. dU_I is formulated by merging the probability and Eq. (3.20) to obtain the function of the angular distribution of the molecular flux emitted from the nozzle. The number of molecules reflected in the $\vec{k}$-direction on a unit area dU_I consequently can be expressed as follows:

$$\begin{aligned} dU_I(\theta) &= p(t,\lambda_m)\rho_f(z)\,cos(\alpha)\,rd\varphi dz \\ &= p(t,\lambda_m)\rho_f(z)\,sin(\theta)\,cos(\varphi)\;rd\varphi dz \end{aligned} \tag{3.22}$$

When the total number of molecules reflected in the $\vec{k}$-direction after colliding with the inner wall of the nozzle is defined as $U_I(\theta)$, $U_I(\theta)$ can be derived as shown below.

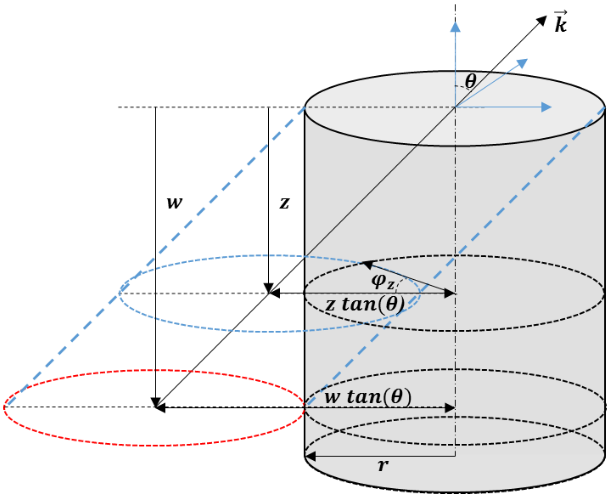

Fig. 3−7. The range of the inner wall of nozzle $2\varphi_z$ at position z in which the reflected molecules can be emitted toward the nozzle outlet in the $\vec{k}$−direction

$$U_I(\theta) = \int_0^w \int_{-\varphi_z}^{\varphi_z} p(t, \lambda_m)\rho_f(z) sin(\theta) cos(\varphi)\, r\, d\varphi\, dz \qquad (3.23)$$

Here, w and φ_z indicate the range of the inner wall of the nozzle from which the reflected molecules can be emitted toward the nozzle outlet in the $\vec{k}$−direction. As shown in Fig. 17, the range of the inner wall of the nozzle is the inner wall of nozzle that could be exposed when the nozzle outlet is viewed from the $\vec{k}$−direction. The molecules reflected in the $\vec{k}$−direction after colliding with the other inner wall without this range would collide with the other inner wall of the nozzle, with a different possibility of being emitted onto the inner wall. The virtual circle identical to the nozzle radius moving in the $\vec{k}$−direction is shown on Fig. 17 to express φ_z in the range in which the molecules can be emitted in the $\vec{k}$−direction toward the nozzle outlet at position z.

The angle of φ_z is that between the line connecting centers of two circle and the line connecting the center of the cross-section of the nozzle with regard to the $x - y$ plane at a position z and the intersection of two circles.

The distance between the centers of two circles can be calculated by means of $ztan(\theta)$ and $rcos(\varphi_z)$ as well. Thus, the relationship of Eq. (3.24) holds between the two equations.

$$z\,tan(\theta) = 2rcos(\varphi_z) \tag{3.24}$$

w is the length between the nozzle outlet and the position where two circles come into contact at a point. The value of w can be calculated by the equation $\varphi_z = 0°$,

In the case of $tan(\theta) > \frac{2r}{l}$, there is the case where two circles meet at one point, and w is as follows:

$$w\,tan(\theta) = 2r \tag{3.25}$$

In the case of $tan(\theta) \le \frac{2r}{l}$, however, two circles still have two points at the intersection, even though the virtual circle has reached the end of the nozzle length at the nozzle inlet. In this case, w is the same as in Eq. (3.26), and there is CASE II., where the molecules are directly emitted from the nozzle inlet to the outlet.

$$w = l \tag{3.26}$$

Here, r and l are the nozzle radius and the nozzle length, respectively. Eq. (3.23), in which $U_I(\theta)$ represents the number of molecules of CASE I., is derived by using Eq. (3.24) as follows:

$$U_I(\theta) = \int_0^w \int_{-\varphi_z}^{\varphi_z} p(t,\lambda_m)\rho_f(z)\,sin(\theta)\,cos(\varphi)\,rd\varphi dz$$
$$= 2rsin(\theta)\int_0^w p(t,\lambda_m)\rho_f(z)sin(\varphi_z)\,dz \tag{3.27}$$

When the MFP of the molecules inside the nozzle is λ_m, the probability $p(\theta, z, \lambda_m)$ that the molecules travel as a distance t without a collision satisfies the exponential function. [18] [23]

$$p(t,\lambda_m) = exp\left(-\frac{t}{\lambda_m}\right) \tag{3.28}$$

The density of the molecules enter the nozzle inlet can be expressed by MFP λ_m. When the molecules with the molar mass M, the temperature T enter the nozzle inlet as much as the molecular inflow $\dot{m}\,g/h$, MFP λ_m of Eq. (3.1) can be re-described as shown as Eq. (3.29). [24]

$$\lambda_m = \frac{1}{\sqrt{2}\pi d^2 n_v} = \frac{1}{\sqrt{2}\pi d^2}\frac{r^2\sqrt{8\pi k_B MT}}{\dot{m}} = \frac{2r^2}{\dot{m}d^2}\sqrt{\frac{k_B MT}{\pi}} \tag{3.29}$$

Here, k_B is the Boltzmann constant.

The free travelling distance t of the molecule in the $\vec{k}$-direction at a position z is as follows:

$$t = \frac{z}{cos(\theta)} \tag{3.30}$$

With Eq. (3.24), Eq. (3.26), Eq. (3.28) and Eq. (3.29), The angular distribution of CASE I. $U_I(\theta)$ for the molecules reflected on the inner wall of the nozzle can be derived as shown as Eq. (3.32).

$$U_I(\theta) = 2r\, sin(\theta) \int_0^w exp\left(-\frac{z}{\lambda_m\, cos(\theta)}\right) (az+b) \sqrt{1-\left(\frac{z\, tan(\theta)}{2r}\right)^2}\; dz \tag{3.31}$$

3.3.2. The molecules directly emitted toward the nozzle outlet from the nozzle inlet (CASE II.)

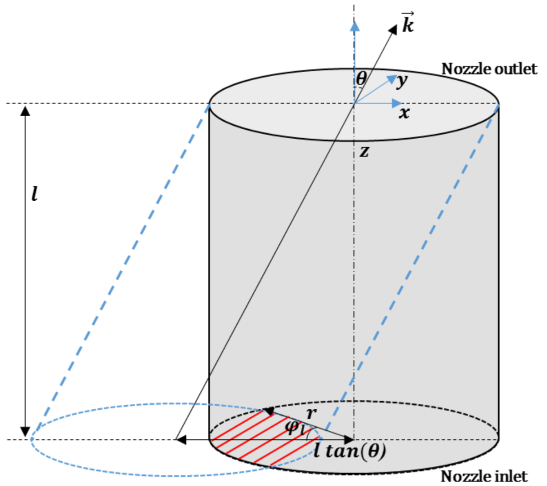

Fig. 3−8. The area on the nozzle inlet where the free molecules can be emitted toward the nozzle outlet in $\vec{k}-$ direction

When $tan(\theta) \leq \frac{2r}{l}$, the virtual circle and the cross-section of the nozzle do not meet at one point, until w reaches the nozzle length l, and the angle φ_l which means φ_z at the position l, is not'zero'. In CASE II., the molecules that can reach the nozzle outlet from the nozzle inlet without colliding with the inner wall of the nozzle outlet. The area where the molecules can be emitted in the $\vec{k}$−direction on the nozzle inlet is identical to the overlap of the two circles at $z = l$ in Fig. 18. The area A can be calculated using φ_l from Eq. (3.24).

$$A = 2\left(r^2\varphi_l - \frac{rl}{2}tan(\theta)sin(\varphi_l)\right) \tag{3.32}$$

The number of molecules directly emitted toward the nozzle outlet $U_{II}(\theta)$ can be obtained by applying the equation used for the number of molecules in the $\vec{k}$−direction, as shown in Fig. 18.

$$U_{II}(\theta) = Ap(t_l, \lambda_m)cos(\theta) \tag{3.33}$$

Here, $p(t_l, \lambda_m) = exp\left(-\frac{t_l}{\lambda_m}\right)$ represents to the probability of the molecules reach the nozzle outlet from the nozzle inlet. The free travelling distance t_l of the molecule in the $\vec{k}$-direction at the nozzle inlet l is by putting $z = l$ into Eq. (3.30).

$$t_l = \frac{l}{cos(\theta)} \tag{3.34}$$

As substituting Eq. (3.34) for t_l of $p(t_l, \lambda_m)$, Eq. (3.35) can be derived.

$$p(t_l, \lambda_m) = exp\left(-\frac{l}{\lambda_m \, cos(\theta)}\right) \tag{3.35}$$

Once Eq. (3.32) and Eq. (3.35). are put into Eq. (3.33), the angular distribution of CASE II. $U_{II}(\theta)$ for the molecules directly emitted toward the nozzle outlet can be re-described as follows.

$$U_{II}(\theta) = 2\,r^2\,exp\left(-\frac{l}{\lambda_m \, cos(\theta)}\right) \cos(\theta)\ \left(\varphi_l - cos(\varphi_l) sin(\varphi_l)\right) \tag{3.36}$$

3.4. Modeling of the Molecules with the Intermolecular Collisions

The CASE I. and CASE II. modeled previous section are the model for the molecules in the free molecular flow are emitted through the nozzle outlet. In these cases, the only condition that can be emitted without collision, is dealt with, except the case in which the molecules can not be emitted by the intermolecular collision.

In order to model the case of the molecules that lost their initial directionality by the intermolecular collision, the longitudinal density of the last intermolecular collisions has been modeled and the case in which the molecules with the intermolecular collisions are emitted toward the nozzle outlet is modeled by using the density.

The approach is same with CASE I. and II. The only difference is the longitudinal density of the last intermolecular collisions is applied instead of the longitudinal density of the free molecular flow by Clausing's equation and all of the molecules in the case is emitted to the nozzle outlet without additional collision.

3.4.1. The molecules with the intermolecular collision reflected on the inner wall of the nozzle (CASE III.)

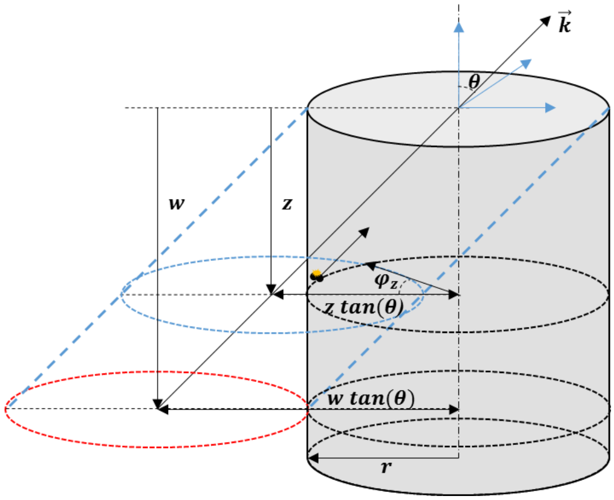

Fig. 3−9. The range of the inner wall of nozzle $2\varphi_z$ at position z in which the reflected molecules with the intermolecular collisions can be emitted in the $\vec{k}$−direction

The angular distribution of CASE III. $U_{III}(\theta)$ is that the molecules with the intermolecular collisions are emitted after reflection on the inner wall of the nozzle. It is the similar as calculation method in CASE I. The longitudinal density of the last intermolecular collisions $\rho_c(z)$, however, is used instead of the longitudinal density of the molecules by Clausing's equation $\rho_f(z)$. Because the intermolecular collisions are the last before emission out of the nozzle outlet, the probability of the molecule travelling distance to the nozzle outlet is"1".

The number of molecules with the intermolecular collisions emitted in the $\vec{k}$−direction from a unit area of the inner wall of the nozzle $dU_{III}(\theta)$ can be expressed as follows:

$$dU_{III}(\theta) = \rho_c(z)\, cos(\alpha)\, rd\varphi dz$$
$$= \rho_c(z)\, sin(\theta)\, cos(\varphi)\; rd\varphi dz \qquad (3.37)$$

Here, $\rho_c(z)$ is the longitudinal density of the last intermolecular collisions mentioned above. The total number of the molecules of CASE III. $U_{III}(\theta)$ is as follows, when the number of the molecules of CASE III. from a unit inner wall of the nozzle $dU_{III}(\theta)$ is integrated for all the areas where the molecules are emitted toward the nozzle outlet in the $\vec{k}$-direction.

$$U_{III}(\theta) = \int_0^W \int_{-\varphi_z}^{\varphi_z} \rho_c(z)\, sin(\theta)\, cos(\varphi)\, r d\varphi dz$$
$$= 2rsin(\theta) \int_0^W \rho_c(z) sin(\varphi_z)\, dz \qquad (3.38)$$

In this case, the area φ_z of the inner wall where the molecules can be emitted in $\vec{k}$-direction at a position z can be obtained by using Eq. (3.24). When putting differentiation of Eq. (3.24) into Eq. (3.38) to integrate Eq. (3.38) in the direction of the nozzle length, Eq. (3.40) can be obtained

$$dz\, tan(\theta) = -2rsin(\varphi_z) d\varphi_z \qquad (3.39)$$

$$U_{III}(\theta) = 2rsin(\theta) \int_{\varphi_0}^{\varphi_w} \rho_c(\varphi_z)\, sin(\varphi_z) \left(-\frac{2r}{tan(\theta)}\right) sin(\varphi_z)\, d\varphi_z$$
$$= -4r^2 cos(\theta) \int_{\varphi_0}^{\varphi_w} \rho_c(\varphi_z) sin^2(\varphi_z) d\varphi_z \qquad (3.40)$$

If substituting φ_z for z by using Eq. (3.24) and Eq. (3.39), Eq. (3.40) can be derived as follows.

$$U_{III}(\theta) = -4r^2 \cos(\theta) \int_{\varphi_0}^{\varphi_w} \left(\alpha \frac{2r\, cos(\varphi_z)}{tan(\theta)} + \beta\right)^3 sin^2(\varphi_z)\, d\varphi_z$$
$$= 4r^2 \cos(\theta) \int_{\varphi_w}^{\varphi_0} \left(\alpha \frac{2r\, cos(\varphi_z)}{tan(\theta)} + \beta\right)^3 sin^2(\varphi_z)\, d\varphi_z \qquad (3.41)$$

The following equation consequently be obtained as keeping deriving.

$$U_{III}(\theta) = 4r^2\, cos(\theta) \frac{1}{480}\Bigg(60 \left(\frac{2r\alpha}{tan(\theta)}\right)^3 sin(\varphi_z) - 10 \left(\frac{2r\alpha}{tan(\theta)}\right)^3 sin(3\varphi_z) -$$
$$6 \left(\frac{2r\alpha}{tan(\theta)}\right)^3 sin(5\varphi_z) + 180 \left(\frac{2r\alpha}{tan(\theta)}\right)^2 \beta\varphi_z - 45 \left(\frac{2r\alpha}{tan(\theta)}\right)^2 \beta\, sin(4\varphi_z) +$$
$$360 \left(\frac{2r\alpha}{tan(\theta)}\right) \beta^2\, sin(\varphi_z) - 120 \left(\frac{2r\alpha}{tan(\theta)}\right) \beta^2\, sin(3\varphi_z) + 240\beta^3 \varphi_z -$$
$$120\beta^3\, sin(2\varphi_z)\Bigg)\Bigg|_{\varphi_w}^{\varphi_0} \qquad (3.42)$$

Here, $\varphi_0 = \frac{\pi}{2}$ is the value of φ_z at the nozzle outlet. As mentioned in CASE I., in the case of $tan(\theta) > \frac{2r}{l}$, the two circles meet at one point within the nozzle length l, φ_w is as follows:

$$\varphi_w = 0 \tag{3.43}$$

In the case of $tan(\theta) \leq \frac{2r}{l}$, $w = l$ as shown in Eq. (3.26) and $\varphi_w = \varphi_l$ can be obtained.

$$\varphi_w = \varphi_l = cos^{-1}\left(\frac{l\,tan(\theta)}{2r}\right) \tag{3.44}$$

3.4.2. The molecules with the intermolecular collision emitted from the cross-section of the nozzle toward the nozzle outlet (CASE IV.)

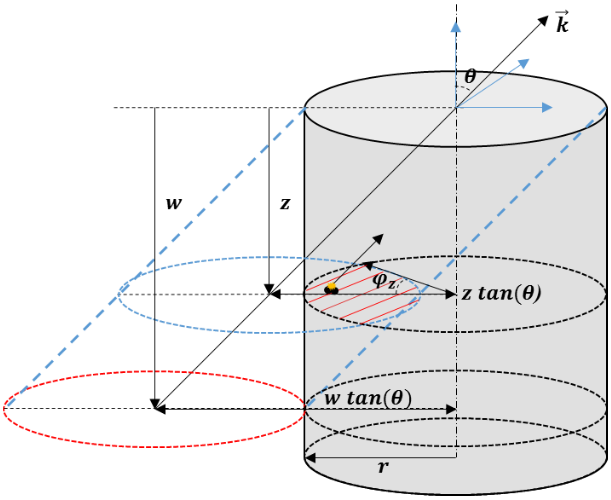

Fig. 3-10. The area in the nozzle where the molecules colliding each other can be emitted toward the nozzle outlet in $\vec{k}$− direction

The molecules with the intermolecular collisions in the nozzle are not only emitted after reflection on the inner wall of the nozzle such as CASE III., but these are directly emitted toward the nozzle outlet after colliding each other. These molecules are covered in CASE IV.

It is assumed that the molecules with the intermolecular collisions follow the law of the energy conservation and the momentum conservation and have no rotation and vibration as a hard sphere. The molecules still follow the Knudsen's cosine law due to the molecules enter the nozzle inlet with Knudsen's cosine law.

Thus the molecules with the intermolecular collision emitted from the cross-section of the nozzle $dU_{IV}(\theta)$ can be calculated in a similar way to CASE II.

$$dU_{IV}(\theta) = \rho_c(z)\, A(\theta, \varphi_z)\, cos(\theta) dz \tag{3.45}$$

Since the molecules in CASE IV. exist everywhere inside the nozzle, the molecules are integrated in the longitudinal direction such as the molecules of CASE I.

$$U_{IV}(\theta) = cos(\theta) \int_0^w \rho_c(z)\, A(\theta, \varphi_z) dz \tag{3.46}$$

If substituting φ_z for z of Eq. (3.46) by using Eq. (3.24) and Eq. (3.39), Eq. (3.47) can be obtained.

$$U_{IV}(\theta) = cos(\theta) \int_{\varphi_0}^{\varphi_w} \rho_c(\varphi_z)\, A(\theta, \varphi_z) \left(-\frac{2r}{tan(\theta)}\right) sin(\varphi_z)\, d\varphi_z \tag{3.47}$$

The area of the cross-section of the nozzle at the position z where the molecules can be emitted in the $\vec{k}$-direction $A(\theta, \varphi_z)$ can be calculated in a similar way to Eq. (3.32).

$$\begin{aligned} A(\theta, \varphi_z) &= 2\left(r^2 \varphi_z - \frac{r\,z}{2}\, tan(\theta)\, sin(\varphi_z)\right) \\ &= 2r^2(\varphi_z - cos(\varphi_z) sin(\varphi_z)) \end{aligned} \tag{3.48}$$

Eq. (3.47) can be summarized as follows by substituting the density of the last intermolecular collisions, Eq. (3.9) and the area, Eq. (3.48),

$$U_{IV}(\theta) = \tag{3.49}$$

$$\left(-\frac{4r^3}{tan(\theta)}\right) cos(\theta) \int_{\varphi_0}^{\varphi_w} \left(\alpha \frac{2r\, cos(\varphi_z)}{tan(\theta)} + \beta\right)^3 (\varphi_z - cos(\varphi_z)\, sin(\varphi_z))\, sin(\varphi_z)\, d\varphi_z$$

$$= \left(\frac{4r^3}{tan(\theta)}\right) cos(\theta) \int_{\varphi_w}^{\varphi_0} \left(\alpha \frac{2r\, cos(\varphi_z)}{tan(\theta)} + \beta\right)^3 (\varphi_z\, sin(\varphi_z) - cos(\varphi_z)\, sin^2(\varphi_z)) d\varphi_z$$

The equation Eq. (3.50) can finally be obtained as organizing Eq. (3.49).

$$U_{IV}(\theta) = \frac{4}{1920} \frac{r^3 cos(\theta)}{tan(\theta)} \Bigg[10\left(\frac{2r\alpha}{tan(\theta)}\right)^3 sin(6\varphi_z) - 60\left(\frac{2r\alpha}{tan(\theta)}\right)^3 \varphi_z\, cos(4\varphi_z) -$$

$$120\left(\frac{2r\alpha}{tan(\theta)}\right)\left(\left(\frac{2r\alpha}{tan(\theta)}\right)^2 + 6\,\beta^2\right)\varphi_z + 90\left(\frac{2r\alpha}{tan(\theta)}\right)\left(\left(\frac{2r\alpha}{tan(\theta)}\right)^2 + 8\,\beta^2\right) sin(2\varphi_z)$$

$$+45\left(\frac{2r\alpha}{tan(\theta)}\right)\left(\left(\frac{2r\alpha}{tan(\theta)}\right)^2 + 4\beta^2\right) sin(4\varphi_z) + 720\beta\left(\left(\frac{2r\alpha}{tan(\theta)}\right)^2 + 2\beta^2\right) sin(\varphi_z)$$

$$+40\beta\left(7\left(\frac{2r\alpha}{tan(\theta)}\right)^2 + 4\beta^2\right) sin(3\varphi_z)$$

$$-240\left(\frac{2r\alpha}{tan(\theta)}\right)\left(\left(\frac{2r\alpha}{tan(\theta)}\right)^2+6\beta^2\right)\varphi_z\,cos(2\varphi_z)$$

$$-480\beta\left(3\left(\frac{2r\alpha}{tan(\theta)}\right)^2+4\beta^2\right)\varphi_z\,cos(\varphi_z)+72\left(\frac{2r\alpha}{tan(\theta)}\right)^2\beta\,sin(5\varphi_z)$$

$$-480\left(\frac{2r\alpha}{tan(\theta)}\right)^2\beta\varphi_z\,cos(3\varphi_z)\Big]\Big|_{\varphi_w}^{\varphi_0} \tag{3.50}$$

Here, $\varphi_0=\frac{\pi}{2}$ is the value of φ_z at the nozzle outlet. The value of φ_w is Eq. (3.43) and Eq. (3.44) according to the condition of $tan(\theta)$.

Chapter 4. Results & Analysis

4.1. Results of the New Model

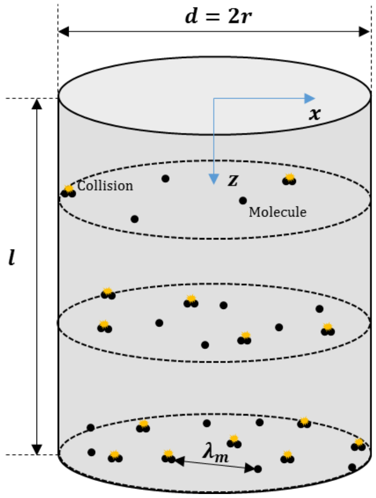

Fig. 4−1. The molecules with the mean free path λ_m in a cylindrical nozzle with the radius r and the length l

The new model for the angular distribution of the molecular flux from a cylindrical nozzle in this paper can be expressed as the sum of all cases in Chapter 3.

$$U(\theta) = U_I(\theta) + U_{II}(\theta) + U_{III}(\theta) + U_{IV}(\theta) \quad (4.1)$$

Using the new model, it is possible to model not only the design of the nozzle, such as the radius and length of the nozzle, but also the angular distribution according to the change in mean free path for the molecular inflow which represents the molecular density in the nozzle.

In order to compare the new model for the angular distribution with DSMC and experiment, the simulation for two types of the cylindrical nozzles where the nozzle diameter is smaller than the nozzle length and the nozzle diameter is larger than the nozzle length.

4.1.1. The cylindrical nozzle (d: $\phi 16$, l: $30mm$)

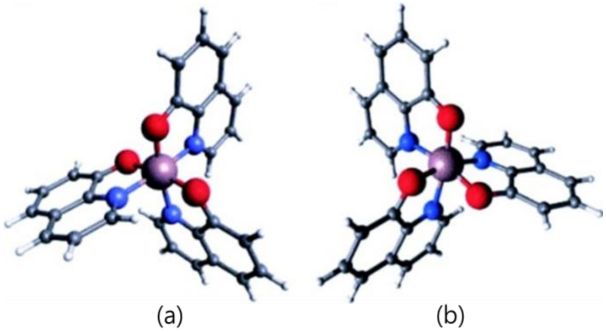

Fig. 4−2. The molecular structure of Alq_3
(a) meridional; (b) facial (violet, Al; red, O; blue, N; Cölle & Brütting 2004)

First, the nozzle diameter is smaller than the nozzle length. When the nozzle diameter (d) and the nozzle length (l) are $\phi 16$ and $30mm$, respectively, the change of the angular distribution according to the change of the molecular inflow (the molecular density) is modeled. In this study, the angular distribution is gotten by using the nozzle, mean free path, and Clausing's equation normalized by the nozzle radius.

Alq_3, a commonly used in OLED manufacturing are used as the molecules. [25] [26] The structure of Alq_3 is shown in Fig. 4−2, but all the molecules in this study are assumed to be a sphere. The properties of Alq_3 are shown in Table. 4−1. [27]

For the cylindrical nozzle with a radius of $8mm$ and a length of $30mm$, each molecular inflow is as shown in Table. 4−2, the normalized values are the values in parentheses.

Table 4−1. The properties of Alq_3

Alq_3		$[unit]$
Mass	7.6292e−22	$[g]$
Diameter	8.4	[Å]
Density	1.31	$[g/cm^3]$
Temperature	500	$[K]$

Table 4-2. The parameters by the molecular inflow into the nozzle (d: $\phi 16$, l: $30mm$) for the new model

Inflow $[g/hr]$	0.167	0.831	0.96	1.68
Radius $[mm]$	8 (1)	8 (1)	8 (1)	8 (1)
Length $[mm]$	30 (3.75)	30 (3.75)	30 (3.75)	30 (3.75)
M.F.P $[mm]$	160.1 (20.0)	32.2 (18.6)	27.8 (4.0)	15.9 (1.99)
K_n	10.0	2.01	1.74	0.99
$a\ for\ \rho_f(z)$	0.176	0.176	0.176	0.176
$b\ for\ \rho_f(z)$	0.17	0.17	0.17	0.17
$\alpha\ for\ \rho_c(z)$	0.0972	0.0788	0.0732	0.0509
$\beta\ for\ \rho_c(z)$	0.0107	0.2824	0.3201	0.4498

The angular distribution by the new model in this study is determined by using normalized values in parentheses.

The parameters for each molecular inflow such as the mean free path, Knudsen number, a and b for the free molecular density by Clausing's equation, and α and β for the last intermolecular collision density are shown in Table. 4-2.

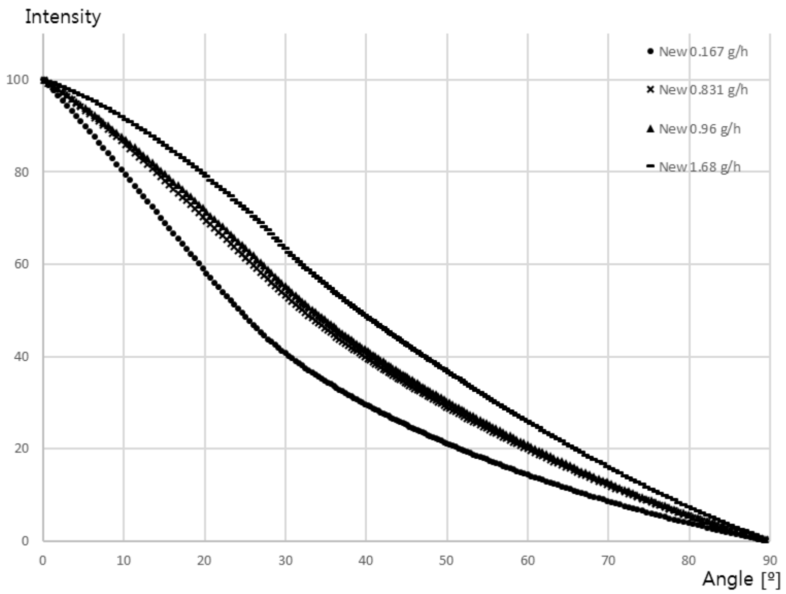

Fig. 4-3. The angular distribution from the nozzle (d: $\phi 16$, l: $30mm$) by the new model

The angular distribution in Fig. 4-3 can be obtained by putting theses parameters into the new model. The shorter mean free path and the smaller Knudsen number mean that the molecules in the nozzle increase, cause the more intermolecular collisions, and consequently make the angular distribution spread.

4.1.2. The cylindrical nozzle (d: $\phi 30$, l: $16mm$)

Table 4−3. The parameters by the molecular inflow into the nozzle (d: $\phi 30$, l: $16mm$) for the new model

Inflow $[g/hr]$	0.08	0.313	0.94	1.566	3.13
Radius $[mm]$	15 (1)	15 (1)	15 (1)	15 (1)	15 (1)
Length $[mm]$	16 (1.07)	16 (1.07)	16 (1.07)	16 (1.07)	16 (1.07)
M.F.P $[mm]$	11750 (783)	300 (20.0)	100 (6.67)	60 (4.00)	30.0 (2.00)
K_n	391.7	10.0	3.33	2.00	1.00
a for $\rho_f(z)$	0.3398	0.3398	0.3398	0.3398	0.3398
b for $\rho_f(z)$	0.3188	0.3188	0.3188	0.3188	0.3188
α for $\rho_c(z)$	0.0163	0.0542	0.0747	0.0844	0.0939
β for $\rho_c(z)$	0.0264	0.0897	0.1294	0.1534	0.1933

The following is the case when the diameter of the nozzle is longer than the length of the nozzle. For cylindrical nozzle with a radius of $15mm$ and a length of $16mm$, the change of the angular distribution of the molecular flux from the nozzle is modelled.

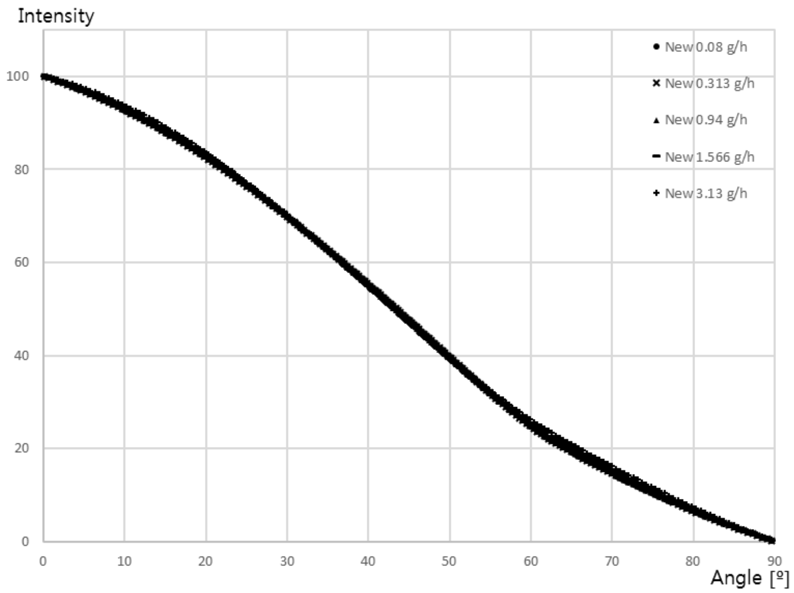

Fig. 4−4. The angular distribution from the nozzle (d: $\phi 30$, l: $16mm$) by the new model

When the parameters for each molecular inflow such as the mean free path, Knudsen number, a and b for the free molecular density by Clausing's equation, and α and β for the last intermolecular collision density are shown in Table. 4-3, the normalized values are in parentheses.

The angular distribution in Fig. 4-3 can be obtained by substituting theses parameters. It can be seen that for the nozzle whose diameter is longer than the length of the nozzle, the angular distribution from the nozzle rarely change.

4.2. Comparison with Results by DSMC

4.2.1. The cylindrical nozzle (d: $\phi 16$, l: $30mm$)

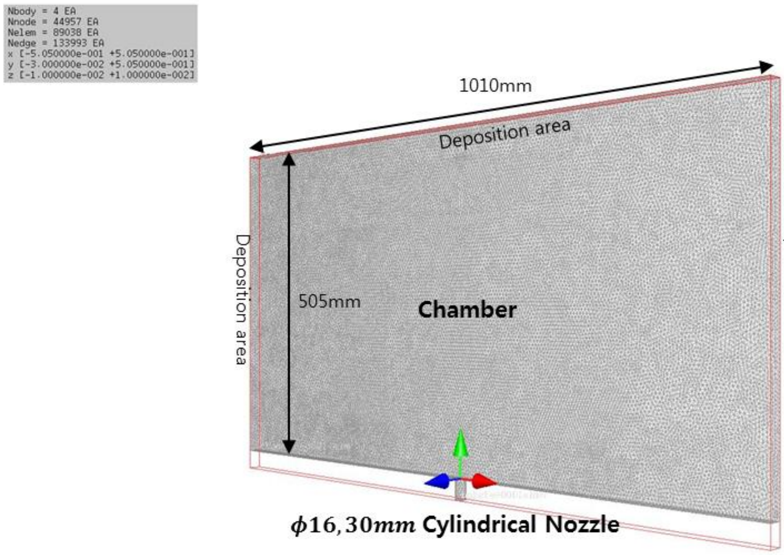

Fig. 4−5. The design of the cylindrical nozzle (d: $\phi 16$, l: $30mm$) and the chamber for DSMC

The angular distribution obtained using the new model is compared to the angular distribution obtained through the DSMC to verify the new model. The molecule used for the simulation is Alq_3 such as that used in the new model. In DSMC, the molecules are assumed the hard sphere same as in the new model, but the simulation is performed after setting it to the various hard sphere. It is assumed that there is no vibration and rotation because the vibration and rotation of the molecules cannot be accurately predicted by LS.

To identify the angular distribution of the molecular flux through the cylindrical nozzle with the radius $8mm$ and the length $30mm$, the chamber where the molecules are deposited and the nozzle are designed to simulate the angular distribution of the molecular flux.

Table 4-4. The simulation conditions of DSMC for the cylindrical nozzle ($\boldsymbol{d}$: $\boldsymbol{\phi 16}$, $\boldsymbol{l}$: $\boldsymbol{30mm}$)

Nozzle		$[\boldsymbol{unit}]$
Cell	404 x 202 x 8	
Element in cell	4367040	
Create particle number	5	$[\#/\boldsymbol{step}]$
Time	20	$[\boldsymbol{s}]$
Time step	1.858388e-06	$[\boldsymbol{s}]$
Simulation time per step	67 ~ 73	$[\boldsymbol{s}]$
Total simulation time	20.95	$[\boldsymbol{hr}]$

As shown in Fig. 4-5, the chamber with the height $505mm$, the length $1010mm$ and the width $20mm$ and the nozzle with the radius $8mm$ and the length $30mm$ are designed to perform DSMC. The plane on which the molecules are deposited is set to three sides except for the one on which the nozzle is located to verify the angular distribution with entire range of $0°$ to $90°$.

Samadii^{TM}/sciv of Metariver Technology Co., ltd is used as DSMC simulation. [28] DSMC is performed to identify the change of the angular distribution with the molecular inflow by designing a space on which the molecules are deposited and the nozzle as shown in Fig. 4-5. The deposition time for the verification of the angular distribution is $20sec$, and it takes $67sec$ to $73sec$ to simulate, regardless of the change of the molecular inflow.

The total time taken for the simulation is as shown in Table. 4-4. For the DSMC, it takes approximately 21 hours to perform DSMC enough to get the reasonable results of the angular distribution. It takes dramatically much time compared to the analytical model, which takes several seconds to simulate.

The molecular inflow used for the simulation and the corresponding mean free path, Knudsen number, and the type of flow are shown in Table 4-5.

Table 4-5. The type of flow, Knudsen number, and mean free path by the molecular inflow into the nozzle ($d{:}\,\phi 16,\ l{:}\,30mm$)

Inflow $[g/hr]$	MFP $[mm]$	K_n	Flow
0.167	160.11	10.01	Free Molecular
0.831	32.17	2.01	Transitional
0.96	27.85	1.74	Transitional
1.68	15.92	0.99	Transitional
2.786	9.60	0.60	Transitional
3.82	7.00	0.44	Transitional
5.34	5.01	0.31	Transitional
8.9	3.00	0.18	Transitional

The angular distribution by each molecular inflow is as shown in Fig. 4-6. There is no more change of the angular distribution by the molecular inflow greater than $1.68g/h$, that is, Knudsen number is less than 1.0. Based on this, the new model in this paper shows that only the angular distribution is considerable, when the Knudsen number is 1.0 or higher.

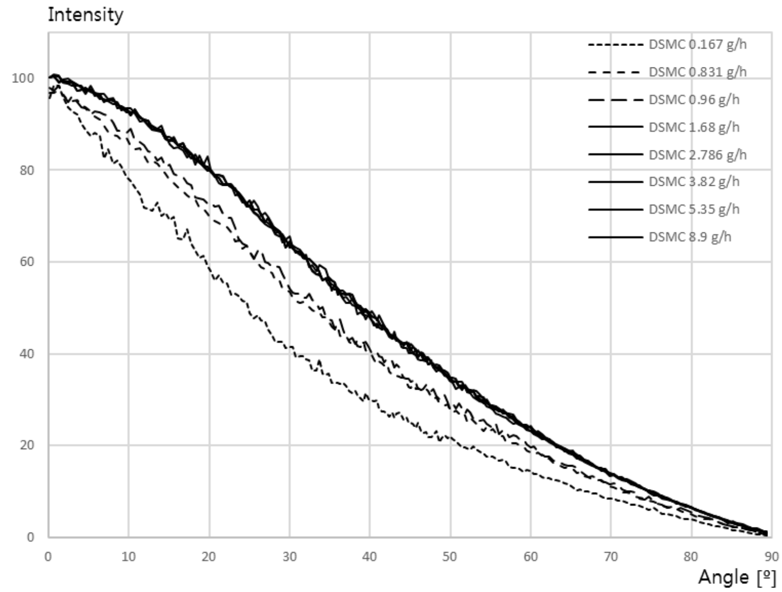

Fig. 4-6. The angular distribution from the nozzle ($d{:}\,\phi 16\,,l{:}\,30mm$) by DSMC

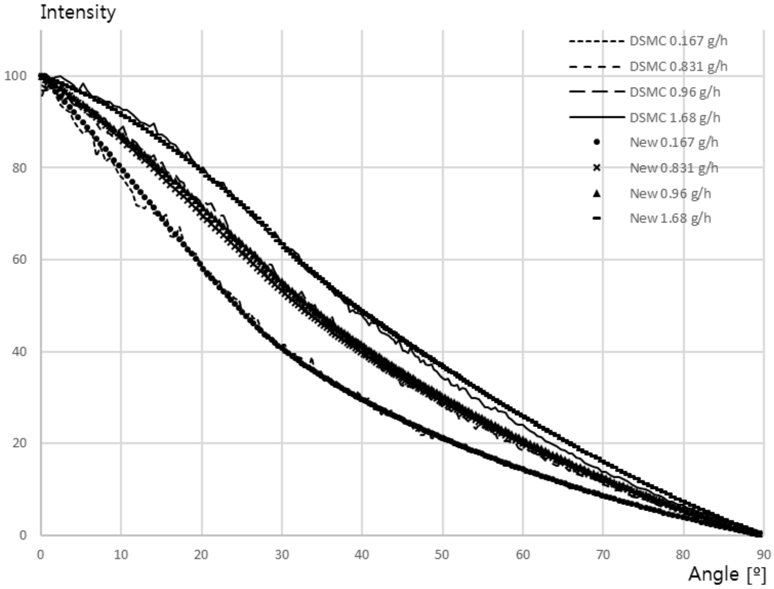

Fig. 4-7. The comparison of the angular distribution from the nozzle ($\boldsymbol{d}$: $\boldsymbol{\phi 16}$, $\boldsymbol{l}$: $\mathbf{30}\boldsymbol{mm}$) by the new model and DSMC

The validity of the new model was verified by comparing the results of DSMC with the results of the new model. The graph in Fig. 4-7 shows the comparison of the two results, in the case of the higher Knudsen number than 1.0. When the two results are compared, the error between the angular distribution obtained by the new model and DSMC expressed as NRMSE is shown in Table 4-6. For each molecular inflow, it can be seen that the results by the two models match within 2.0%.

The error squared between the results of the new model and DSMC for each angle is as shown in Fig. 4-8. The main reason for the large error at the low molecular inflow $0.167 g/h$ is that with a constant simulation time, the number of the molecules calculated in the simulation is not enough, even if the number of molecules existing in the simulations is saturation.

Table 4-6. NRMSE of the new model to DSMC

Inflow $[g/hr]$	0.167	0.831	0.96	1.68
NRMSE [%]	1.749	1.325	1.603	1.958

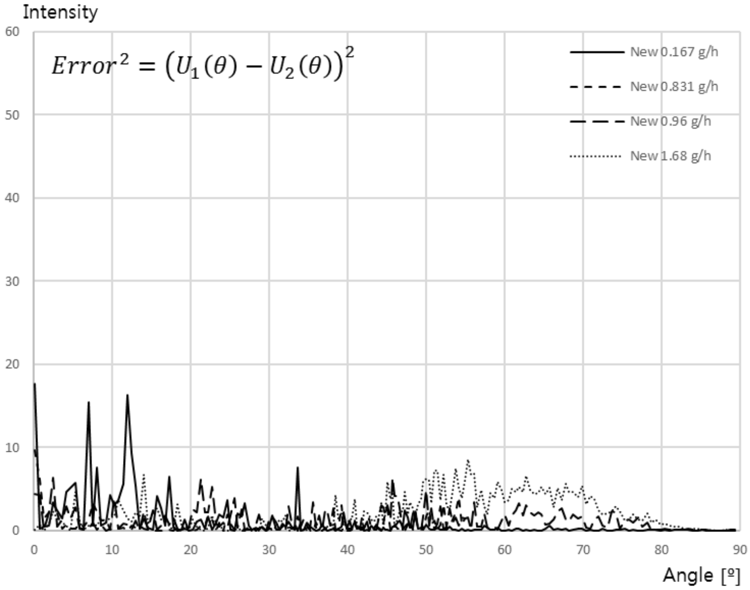

Fig. 4−8. The error squared between the angular distribution from the nozzle ($\boldsymbol{d}$: $\boldsymbol{\phi 16}$, $\boldsymbol{l}$: $\boldsymbol{30mm}$) by the new model and DSMC

4.2.2. The cylindrical nozzle (d: $\phi 30$, l: $16mm$)

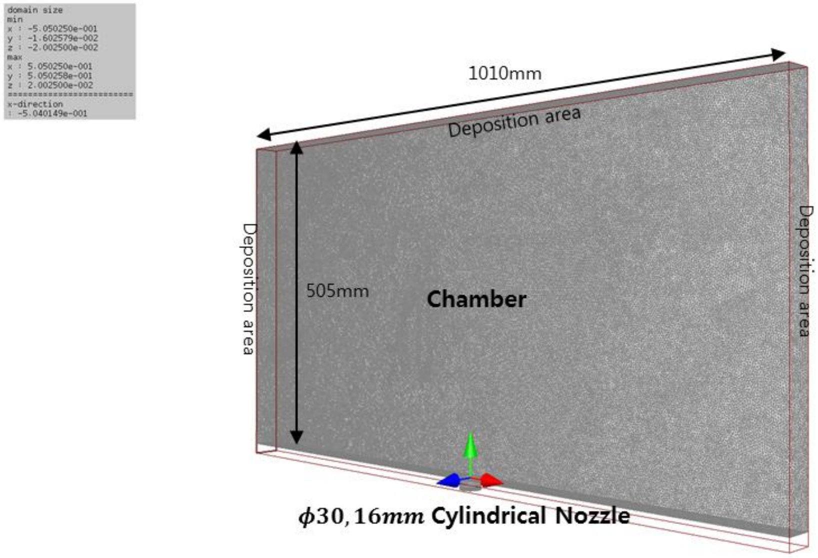

Fig. 4−9. The design of the cylindrical nozzle (d: $\phi 30$, l: $16mm$) and the chamber for DSMC

DSMC is performed to verify the angular distribution from the nozzle with the longer diameter than the length (d: $\phi 30$, l: $16mm$) by the new model. The molecule is Alq_3 as the same molecule used in the new model. In DSMC, the properties of the molecule is the same as the properties in the simulation in 4.2.1. The nozzle and the space where the molecules are deposited are designed as shown in Fig. 4−9 to obtain the angular distribution from the nozzle with the diameter, $\phi 30$ and the length, $16mm$.

Table 4−7. The simulation conditions of DSMC for the cylindrical nozzle (d: $\phi 30$, l: $16mm$)

Nozzle		[***unit***]
Cell	404 x 202 x 16	
Element in cell	9517931	
Create particle number	5	[#/***step***]
Time	20	[***s***]
Time step	1.858388e-06	[***s***]
Simulation time per step	110 ~ 130	[***s***]
Total simulation time	34.59	[***hr***]

Table 4−8. The type of flow, Knudsen number, and mean free path by the molecular inflow into the nozzle (d: $\phi 30$, l: $16mm$)

Inflow $[g/hr]$	MFP $[mm]$	K_n	Flow
0.08	1175.04	39.17	Free Molecular
0.313	300.33	10.01	Free Molecular
0.94	200.01	6.67	Transitional
1.566	100.00	3.33	Transitional
3.13	60.03	2.00	Transitional
4.70	30.03	1.00	Transitional

The simulation time is set $20s$ for obtaining the definite angular distribution, and it takes about $110s$ to $130s$ per a step, regardless of the change in the molecular inflow. The total time taken for the complete of the simulation is as shown in Table. 4-7. For the DSMC, the simulations take approximately $34.6hr$ to get the relatively definite angular distribution could be fully understood.

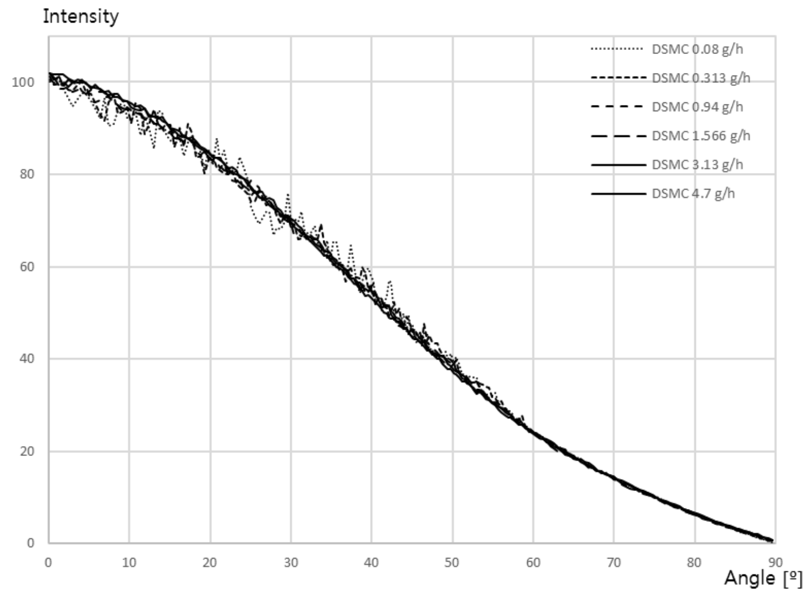

Fig. 4-10. The angular distribution from the nozzle (d: $\phi 30$, l: $16mm$) by DSMC

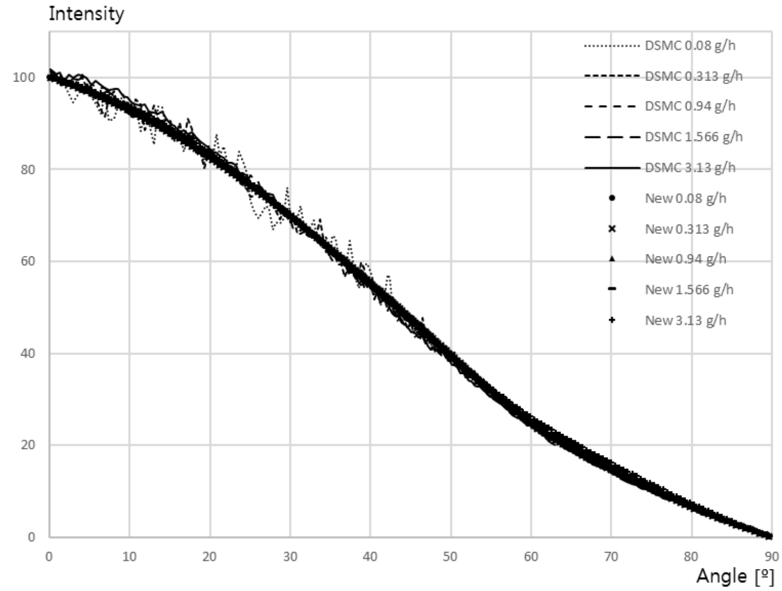

Fig. 4−11. The comparison of the angular distribution from the nozzle $(\boldsymbol{d}: \boldsymbol{\phi 30}, \boldsymbol{l}: \mathbf{16}\boldsymbol{mm})$ by the new model and DSMC

The molecular inflow used for the simulation and the corresponding mean free path, Knudsen number, and the type of flow are shown in Table 4-8.

The results of the angular distribution for each inflow are shown in Fig. 4-10. When the diameter of the nozzle is larger than the length of the nozzle, as with the results of the new model, it has been found that the variation in the angular distribution by change of the molecular inflow is not significant.

To compare the results of DSMC with the results of the new model, the angular distribution of the two models are as follows. Fig. 4-11 shows a graph of the angular distribution of the molecular flow emitted from the nozzle with a longer diameter of the nozzle than the length of the nozzle for the molecular inflow with **1.0** or higher Knudsen number. When comparing the two results, the errors between the angular distribution by the new model and DSMC, which is expressed in NRMSE are shown in Table 4-6.

Table 4-9. NRMSE of the new model to DSMC

Inflow [g/hr]	0.08	0.313	0.94	1.566	3.13
NRMSE [%]	4.118	2.767	1.994	2.111	2.977

The error squared for each degree by the new model and DSMC is as shown in Fig. 4-12. The main reason for the large error at the low molecular inflow $0.08g/h$ is that the number of the molecules calculated in the simulation is not enough, even if the simulation is performed for $34.6hr$.

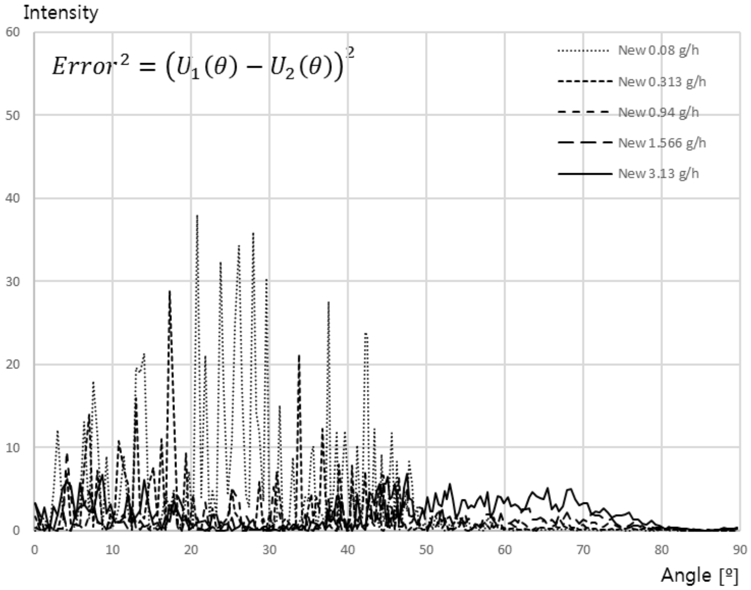

Fig. 4-12. The error squared between the new model and DSMC

4.3. Comparison with results by experiment

4.3.1. Cylindrical nozzle (d: $\phi16$, l: $30mm$)

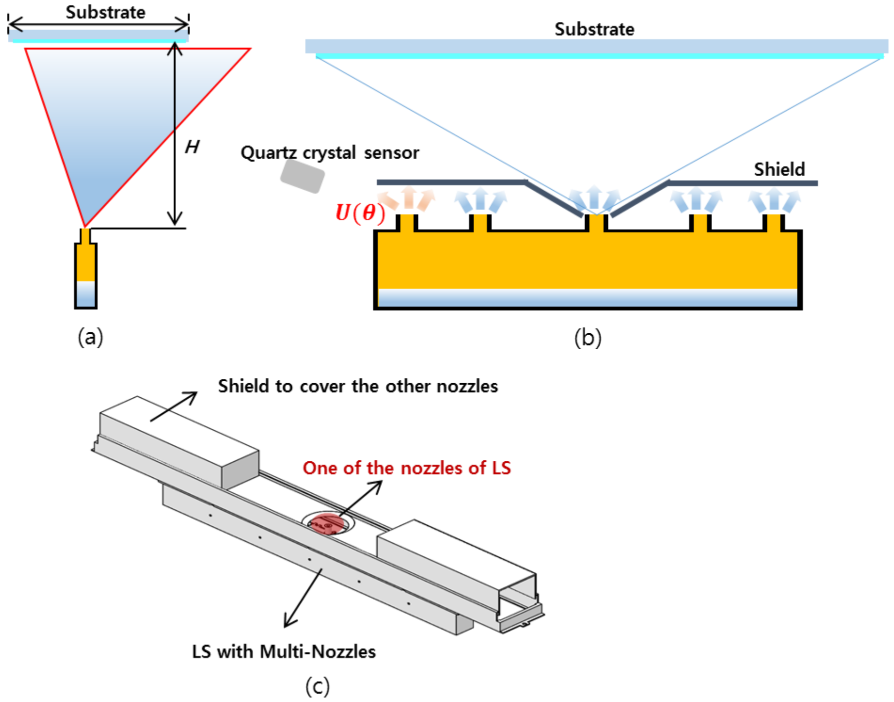

Fig. 4−13. The scheme of experiment
(a) Side view of LS (b) Front view of LS (c) Design of crucible and shield

The experiment is used to validate the new model by comparing with the results of the new model. The experiment is carried out as follows.

First, as using the thickness of the molecules deposited onto a substrate after being emitted from a single nozzle of LS, the angular distribution of the molecules from the nozzle can be valuated. To calculate the angular distribution of the molecule from a single nozzle, the molecules from the other nozzles of LS are blocked up by a shield. The molecular inflow is controlled by a quartz crystal sensor.

Table 4-10. The conditions of the experiment

Material		Alq_3
Nozzle size $[mm]$	Diameter	16
	Length	30
Gap between nozzle and substrate $[mm]$		505
Molecular Inflow $[g/hr]$ (Deposition time $[s]$)		0.167 (3600)
		0.831 (720)
		2.786 (240)

LS is moved and placed under the substrate to perform deposition, after the molecular inflow is kept constant. The conditions of the components of LS used in the experiment are as shown in Table 4-10.

Alq_3 commonly used in OLED manufacture is used in the experiment, and the nozzle with $16mm$ in diameter and $16mm$ in length is used to obtain the angular distribution of the molecule emitted from the nozzle. Because the gap between the nozzle and the substrate is long enough to ignore the size of the nozzle, it can be suggested that the molecule is emitted from one point of the nozzle outlet in the new model. The gap between the nozzle and the substrate is $505mm$ long enough for the size of the nozzle.

The hardware composition of this actual experiment is shown in Figure 4-14. to The gap between the nozzle and the substrate is set at $505mm$ far enough; since it is assumed that the gap between the nozzle and the substrate is far from the size of the nozzle and that the molecule is emitted from one outlet of the nozzle.

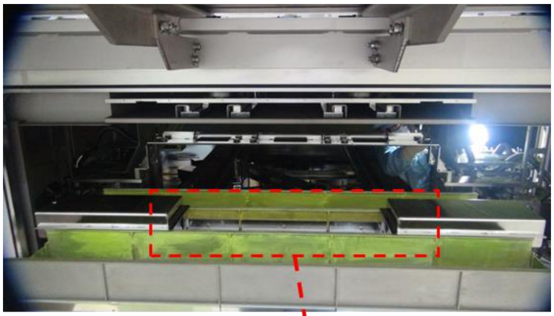

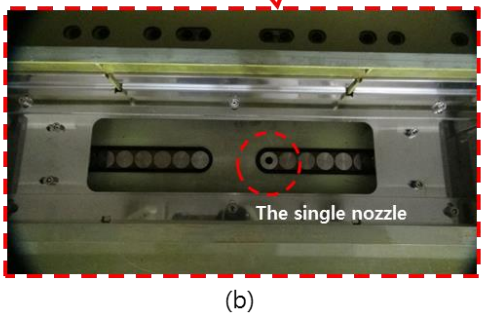

Fig. 4−14. (a) The LS for the experiment (b) The single nozzle of LS

The hardware of LS for the experiment is shown in Fig. 4−14.

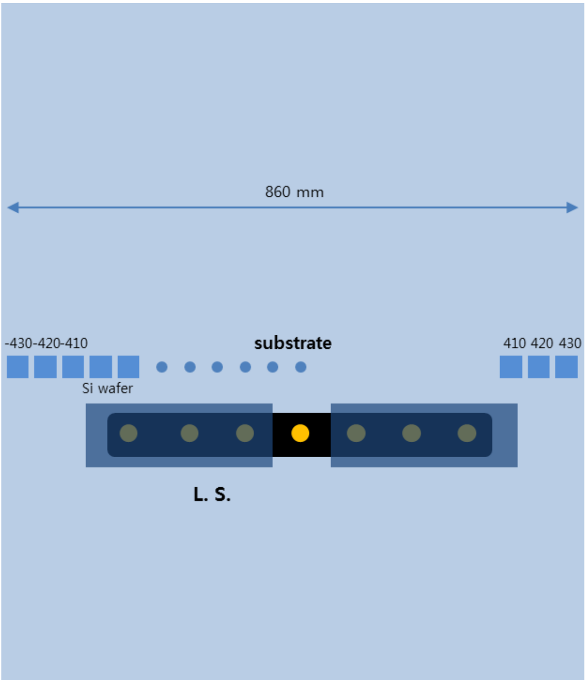

Fig. 4−15. The position on the substrate where the thickness is measured

Fig. 4-16. Ellipsometer (J. A. Woollam Co., Inc. M-2000 series)

The thickness of Alq_3 deposited on Si wafer is measured and Si wafer attached on the substrate is located in the following position on the substrate as shown in Fig. 4-15.

M-2000 series elipometer of J. A. Woollam is used to measure the thickness of the molecule. The reason why the thickness is measured after depositing on Si wafer is because the thickness can be accurately measured when the model of substrate is set to Si wafer in elipometer.

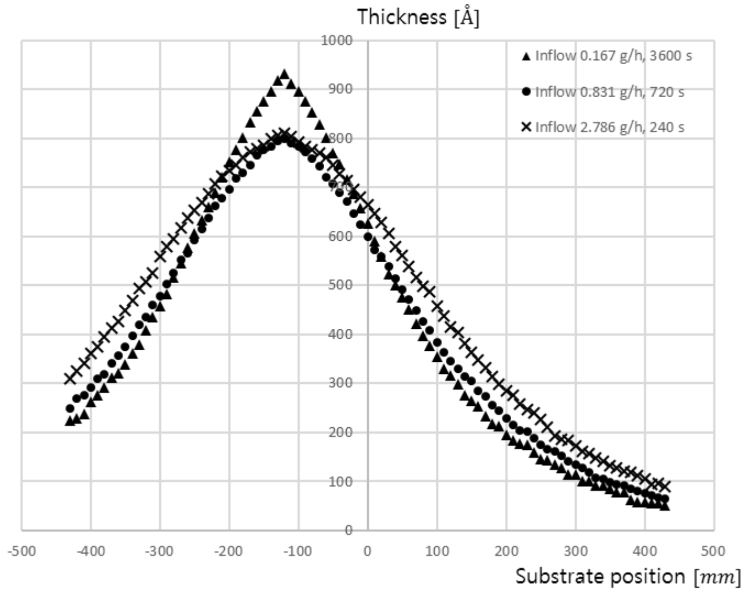

Fig. 4-17. The thickness profile from LS with a single nozzle ($\boldsymbol{d}$: $\boldsymbol{\phi 16}$, $\boldsymbol{l}$: $\boldsymbol{30mm}$)

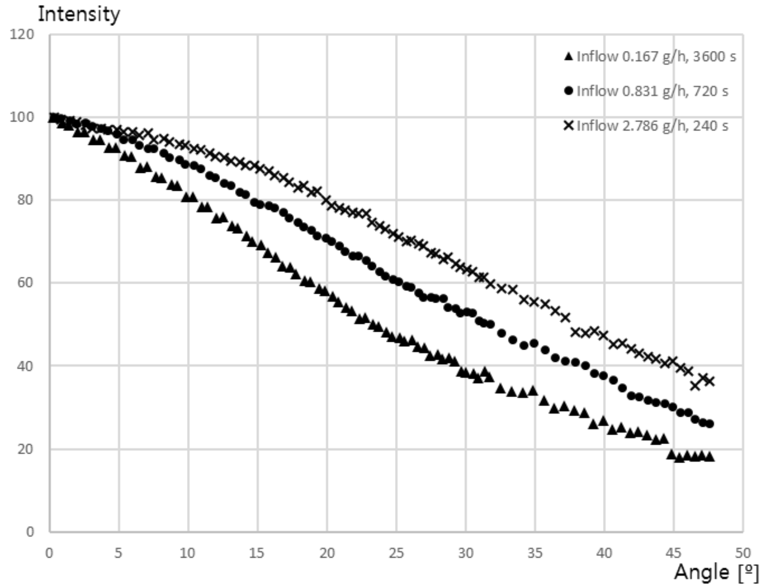

Fig. 4-18. The angular distribution by converting the thickness profile by experiment

When deposition is performed with different molecular inflows, and the thickness of the molecules deposited on the substrate is measured by using elisometer, the thickness profile for each position is as shown in Fig. 4-17. The angular distribution can be converted by Eq. (4.2) as shown in Fig. 4-18.

$$U(\theta) = m\frac{x^2+H^2}{cos(\phi)} \tag{4.2}$$

Mean free path(Knudsen number) for each molecular inflow is 160mm (10.1) at 0.167g/h, 32.17mm (2.01) at 0.831g/h, and 9.6mm(0.60) at 2.786g/h. The lower molecular inflow can cause the more sharp angular distribution.

In order to compare the angular distribution by the experiment and the angular distribution by the new model, the angular distribution by the new model is evaluated as follows. The angular distribution by the new model is derived using the values of man free path 15.92mm, which Knudsen number is 1.00. Because the angular distribution below 1.00 of Knudsen number such as 2.786g/h of the molecular inflow keep constant.

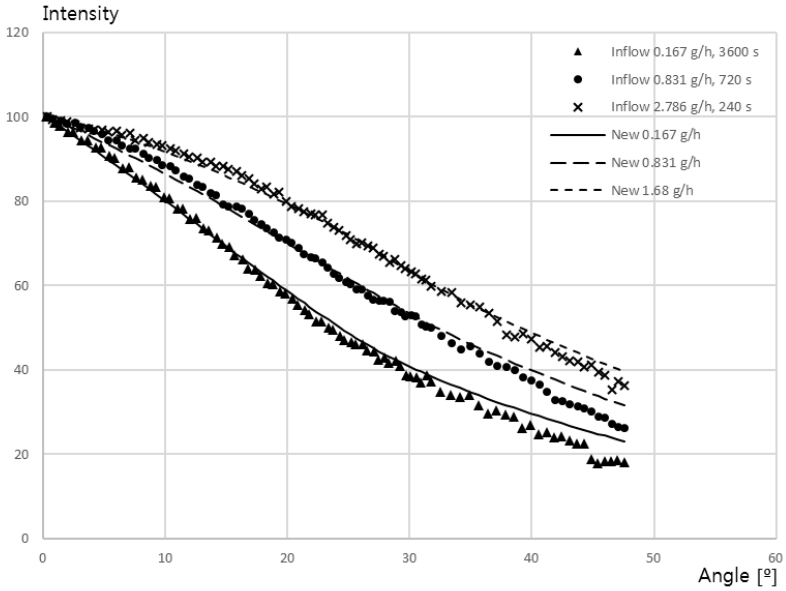

Fig. 4−19. The comparison of the angular distribution from the nozzle $(\boldsymbol{d}{:}\,\boldsymbol{\phi 16}\,, \boldsymbol{l}{:}\,\boldsymbol{30mm})$ by the new model and the experiment

The graph in Fig. 4-19 shows the comparison of two types of the angular distributions evaluated by the experiment and the new model. The error squared between the results of the experiment and the new model for each position is shown in Fig. 4-20.

Compared to the results of DSMC, the difference in the angular distribution at lower angles is larger.

The error of each angular distribution expressed in NRMSE is shown in Table. 4-11. It can be seen that there are large errors in the low molecular inflow and that the higher the inflows, the smaller error becomes. This is because the error in the low angle is greater when it is the low molecular inflow than when it is the high molecular inflow.

To figure out why the error is large in this low angle, the results of the DSMC are compared with the results of the experiment.

Table 4−11. NRMSE of the new model to the experiment

Inflow $[\boldsymbol{g/hr}]$	0.167	0.831	2.786
NRMSE [%]	4.306	3.372	2.004

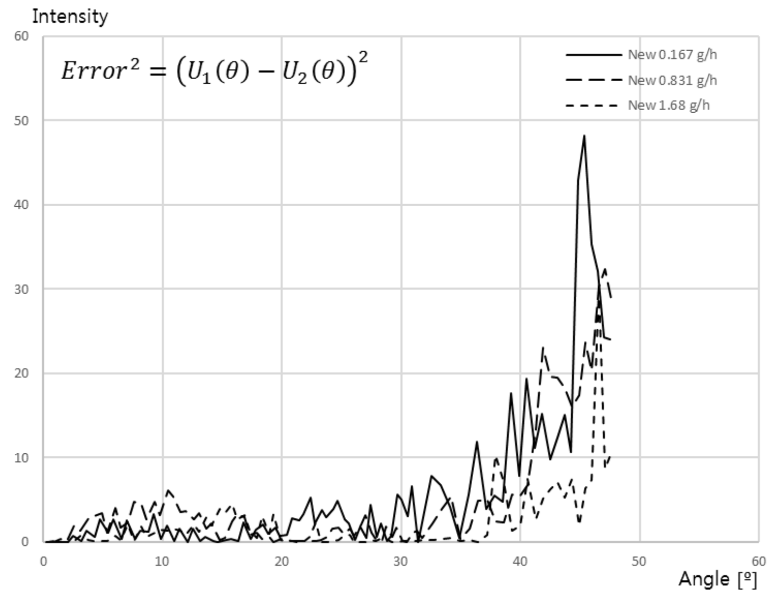

Fig. 4−20. The error squared between the new model and the experiment

Fig. 4-21 shows a comparison of the angular distribution by DSMC and the experiment for a nozzle with $16mm$ in diameter and $16mm$ in length, and the error squared between the two angular distribution is shown in Fig. 4-20.

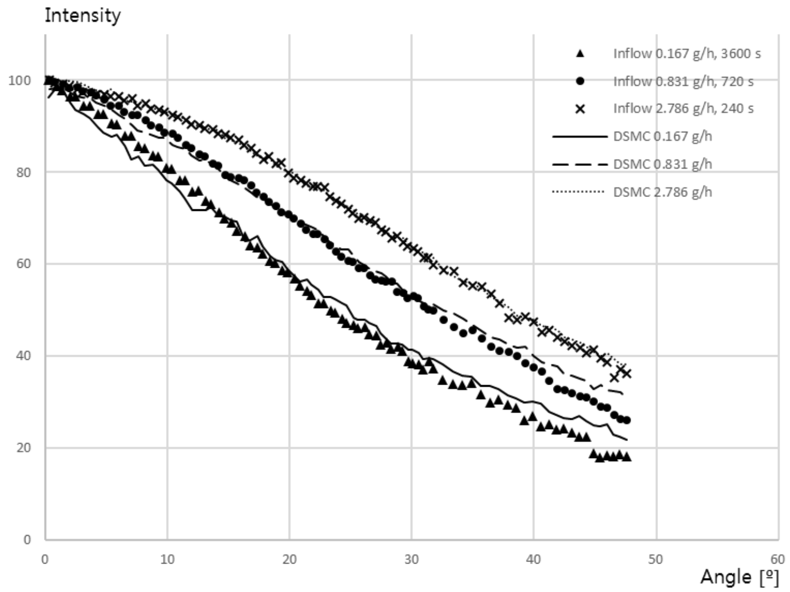

Fig. 4−21. The comparison of the angular distribution from the nozzle $(\boldsymbol{d}: \boldsymbol{\phi 16}, \boldsymbol{l}: \boldsymbol{30mm})$ by DSMC and the experiment

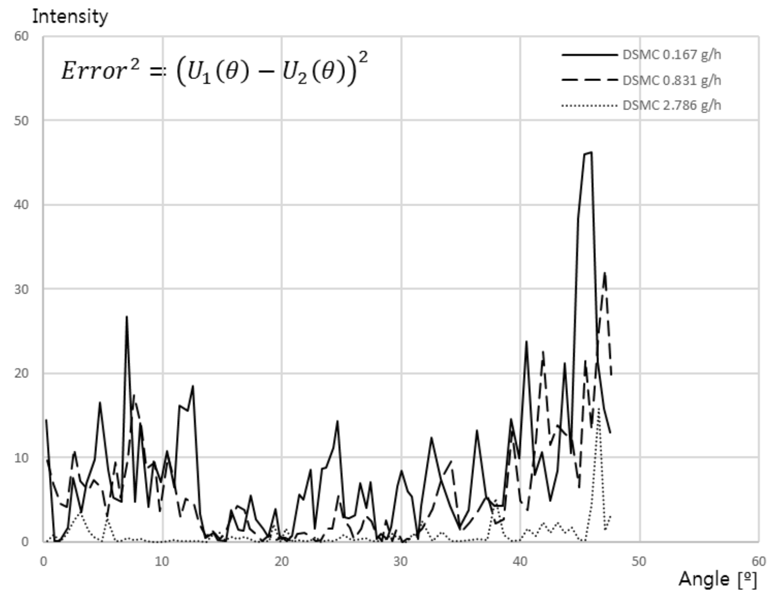

Fig. 4-22. The error squared between DSMC and the experiment

There is large error in the low angle in the comparison between the two angular distributions as well.

NRMSE calculated as **5.21**, **3.676**, and **1.281** also show a large error with the low molecular inflow. This is determined by the error in the measurement that could occur when measuring the film thickness in the experiment. Because the thickness of the thin film being measured is thinner, the error is relatively larger, the larger error is shown in the measurement of the thinner thickness at the high angle and the low molecular inflow.

Table 4-12. NRMSE of DSMC to the experiment

Inflow [g/hr]	0.167	0.831	2.786
NRMSE [%]	5.251	3.676	1.281

Chapter 5. Conclusions

In this paper, the analytical model of the angular distribution of the molecular flux with the intermolecular collisions from a cylindrical nozzle is studied. The results are verified by DSMC and experiment. The results are as follows.

- The molecular density in the nozzle is modelled by the longitudinal density of the free molecular flow by Clausing's equation and the longitudinal density of the last intermolecular collisions.

- The angular distribution by the change of the molecular density in nozzle can be evaluated by using the design of the nozzle such as the radius of the nozzle, the length of the nozzle, and mean free path.

- In this study, when the results of the new model and DSMC for the cylindrical nozzle with 16mm in the diameter and $30mm$ in the length are compared, NRMSE of the angular distribution by the change of the molecular density is evaluated as 1.75%, 1.32%, 1.60%, and 1.96%, respectively.

- In this study, when the results of the new model and DSMC for the cylindrical nozzle with 30mm in the diameter and $16mm$ in the length are compared, NRMSE of the angular distribution by the change of the molecular density is evaluated as 4.12%, 2.77%, 1.99%, and 2.98%, respectively.

- In this study, when the results of the new model and the experiment for the cylindrical nozzle with 16mm in the diameter and $30mm$ in the length are compared, NRMSE of the angular distribution by the change of the molecular density is evaluated as 4.31%, 3.37%, and 2.00%, respectively.

In this study, the analytical model has been suggested how the angular distribution from a cylindrical nozzle, which change with the change of the molecular density, can be predicted without performing any DSMC or experiments. This not only predicts the angular distribution by the change of the design of the nozzle, but also the change of the molecular inflow, i.e. the new model for the angular distribution of the molecular flux from a cylindrical nozzle, thereby, can be expected reducing the simulation time of LS and the optimization of uniformity in a substrate.

APPENDIX

A. The results of new model for the cylindrical nozzle with d: $\phi 16, l$: $30mm$

Table A. The angular distribution by new model (d: $\phi 16, l$: $30mm$)

Intensity

Angle [º]	0.167 g/h	0.831 g/h	0.96 g/h	1.68 g/h
0.1418225	100	100	100	100
0.7090997	98.917869	99.315923	99.378873	99.648831
1.2762379	97.825003	98.617217	98.742847	99.280328
1.8431263	96.722048	97.904421	98.092424	98.894858
2.4096539	95.60966	97.178087	97.428117	98.492806
2.9757094	94.488504	96.438781	96.750455	98.074572
3.5411852	93.359246	95.687074	96.059973	97.640571
4.1059711	92.222567	94.923552	95.357219	97.191232
4.6699589	91.079147	94.148808	94.642749	96.726999
5.2330412	89.929674	93.363439	93.917128	96.248324
5.7951106	88.774843	92.568055	93.180926	95.755671
6.3560641	87.615343	91.763261	92.434717	95.24951
6.9157968	86.451873	90.949673	91.679082	94.73032
7.4742062	85.285132	90.127908	90.914603	94.198585
8.0311912	84.115821	89.298583	90.141864	93.654794
8.5866515	82.944642	88.462319	89.361453	93.09944
9.1404914	81.77229	87.619729	88.573949	92.533013
9.6926139	80.599466	86.771431	87.779938	91.956008
10.242925	79.426868	85.918036	86.98	91.368915
10.791333	78.25519	85.060152	86.174709	90.772224
11.337749	77.08512	84.19838	85.364635	90.166417
11.882075	75.917368	83.33333	84.550356	89.551986
12.424246	74.75258	82.465564	83.732402	88.929382
12.964154	73.591483	81.595697	82.911356	88.299095
13.501741	72.434708	80.724267	82.087726	87.661556
14.036906	71.282973	79.85187	81.262075	87.017236
14.569593	70.1369	78.979025	80.43489	86.366542
15.099708	68.997198	78.106305	79.606712	85.709922
15.627201	67.864477	77.234204	78.778003	85.047754
16.151979	66.739438	76.363271	77.949279	84.380457
16.673999	65.622682	75.493972	77.120973	83.708376
17.193175	64.514901	74.626828	76.293571	83.031895
17.709456	63.416711	73.762293	75.467492	82.351334
18.222794	62.328729	72.900806	74.643141	81.666995
18.73311	61.251636	72.042839	73.820951	80.979195
19.240373	60.186022	71.18878	73.001274	80.288174
19.74451	59.132568	70.339068	72.184507	79.594198
20.245492	58.091869	69.494054	71.370959	78.897449
20.743255	57.06461	68.654138	70.560986	78.198131
21.237773	56.0514	67.819634	69.754854	77.496359
21.728985	55.052942	66.9909	68.95287	76.79226
22.216874	54.069873	66.168205	68.155249	76.085861
22.701383	53.10293	65.351863	67.36224	75.377193
23.182498	52.152799	64.542094	66.573999	74.666167
23.660168	51.220283	63.739153	65.790703	73.952677
24.134383	50.306157	62.943202	65.012427	73.236468
24.605097	49.41134	62.154425	64.239253	72.517224
25.072306	48.53677	61.372896	63.471135	71.79442
25.535968	47.683587	60.598693	62.708	71.067376
25.996081	46.853055	59.831744	61.949592	70.335051
26.45261	46.046796	59.071917	61.195525	69.595986
26.905556	45.266862	58.3188	60.445036	68.84785
27.354888	44.51632	57.571624	59.696793	68.086743
27.800613	43.800631	56.828427	58.947723	67.304338
28.242702	43.137092	56.080657	58.185321	66.468428
28.681166	42.504921	55.341673	57.428412	65.627313
29.11598	41.890832	54.622773	56.69212	64.816133
29.547149	41.294685	53.923337	55.975721	64.032856
29.97468	40.714802	53.241869	55.277731	63.275058
30.398553	40.150893	52.577774	54.597486	62.541091
30.818788	39.602046	51.930093	53.934	61.829178
31.235368	39.067825	51.298219	53.286624	61.137931
31.648316	38.547306	50.681247	52.654443	60.46584
32.057618	38.039784	50.078452	52.036717	59.811633
32.463299	37.545097	49.489464	51.433027	59.174352
32.86535	37.062658	48.913679	50.842758	58.552973
33.263796	36.591865	48.350484	50.265286	57.946505
33.658632	36.132264	47.799396	49.700114	57.354127
34.049885	35.683204	47.259793	49.146621	56.774948
34.437553	35.244726	46.731552	48.604645	56.208508

34.821664	34.815928	46.213905	48.07344	55.653891
35.202219	34.396838	45.706743	47.552864	55.110724
35.579248	33.987176	45.209742	47.042582	54.578494
35.952752	33.586519	44.722503	46.542195	54.056669
36.322766	33.194194	44.244447	46.051138	53.544582
36.689292	32.810308	43.775553	45.569363	53.042043
37.052364	32.434276	43.315312	45.096372	52.548481
37.411988	32.066292	42.863782	44.632194	52.063805
37.768198	31.705427	42.420217	44.17612	51.587286
38.121003	31.352333	41.985013	43.728489	51.119139
38.470438	31.005777	41.557214	43.2884	50.65848
38.816512	30.666572	41.13734	42.856314	50.205657
39.159255	30.333702	40.724598	42.431479	49.759937
39.498698	30.007211	40.318954	42.013848	49.321223
39.834851	29.687044	39.920321	41.603324	48.889389
40.167751	29.372783	39.528334	41.199553	48.464073
40.497412	29.064551	39.143041	40.802565	48.045276
40.823871	28.761928	38.764079	40.412012	47.632649
41.147141	28.464582	38.391163	40.027616	47.225916
41.467261	28.172967	38.024582	39.64963	46.825296
41.784245	27.886628	37.663965	39.277702	46.43045
42.098131	27.605214	37.309004	38.911534	46.041085
42.408935	27.328824	36.959741	38.551153	45.657225
42.716695	27.057319	36.616032	38.196416	45.278728
43.021426	26.79039	36.277614	37.847071	44.905353
43.323167	26.528114	35.944509	37.503125	44.537107
43.621935	26.270372	35.616598	37.164463	44.173883
43.917769	26.016906	35.293653	36.830861	43.815466
44.210684	25.767756	34.975678	36.502316	43.461863
44.50072	25.522568	34.662368	36.178536	43.112792
44.787894	25.281745	34.354014	35.859784	42.768519
45.073723	25.043126	34.048285	35.54372	42.426592
45.376607	24.792275	33.726244	35.210696	42.065643
45.682679	24.540523	33.402551	34.87589	41.702082
45.991983	24.287861	33.077189	34.539283	41.335867
46.304542	24.034296	32.750162	34.200879	40.966985
46.620399	23.779819	32.421454	33.860659	40.595397
46.939575	23.524437	32.091074	33.518632	40.221092
47.262116	23.268142	31.759005	33.17478	39.844033
47.588047	23.011083	31.425365	32.829211	39.464311
47.917395	22.75305	31.089987	32.481771	39.081752
48.250204	22.494089	30.752902	32.132484	38.696362
48.586494	22.234223	30.41413	31.78137	38.308145
48.926308	21.973449	30.073662	31.428418	37.917072
49.269666	21.711781	29.731515	31.073646	37.523143
49.616611	21.449214	29.387678	30.717041	37.12633
49.96716	21.185765	29.042172	30.358623	36.726636
50.321356	20.92143	28.694988	29.998382	36.324038
50.679217	20.656226	28.346147	29.636341	35.918541
51.040783	20.390151	27.995644	29.272492	35.510124
51.406078	20.123218	27.643497	28.906853	35.098791
51.775121	19.855443	27.289723	28.539441	34.684548
52.147955	19.586825	26.934321	28.170256	34.26738
52.52459	19.317386	26.57732	27.799325	33.847304
52.905067	19.047128	26.218721	27.426651	33.424311
53.289397	18.776076	25.858556	27.052265	32.998423
53.677617	18.504232	25.496831	26.676173	32.569635
54.069737	18.231624	25.13358	26.298411	32.137977
54.465792	17.958258	24.768814	25.918987	31.703446
54.86579	17.684162	24.402569	25.537942	31.26608
55.269764	17.409345	24.034861	25.155289	30.825883
55.677718	17.133838	23.66573	24.771073	30.382897
56.089685	16.857653	23.295195	24.38531	29.937133
56.505674	16.580817	22.923296	23.998042	29.488632
56.92569	16.303362	22.550074	23.609314	29.037437
57.349763	16.025303	22.175554	23.219151	28.58357
57.77789	15.746678	21.799791	22.827607	28.12709
58.210095	15.467505	21.422811	22.434714	27.668027
58.646371	15.187826	21.044675	22.040532	27.206447
59.086742	14.907663	20.665415	21.645097	26.742388
59.531195	14.62706	20.285095	21.248475	26.275925
59.979751	14.346042	19.903755	20.850708	25.807103
60.432393	14.064657	19.521464	20.451866	25.336006
60.889138	13.782934	19.138265	20.051998	24.862686
61.349966	13.500923	18.754233	19.651181	24.387238
61.814888	13.218658	18.369419	19.249467	23.909722
62.283889	12.936187	17.983894	18.846934	23.430232
62.756949	12.653563	17.597736	18.443662	22.948866
63.234075	12.370822	17.211003	18.039711	22.465699
63.715234	12.088025	16.823784	17.635177	21.980848
64.200427	11.805214	16.436142	17.230126	21.494396
64.689615	11.522452	16.048174	16.824659	21.00647
65.182795	11.239785	15.659948	16.418849	20.517165
65.679924	10.957281	15.271566	16.012803	20.026615
66.180991	10.674989	14.883103	15.606601	19.534924

66.685948	10.392979	14.494666	15.200356	19.042237
67.194779	10.111306	14.106337	14.794154	18.548668
67.70743	9.8300448	13.718229	14.388113	18.05437
68.223878	9.5492511	13.330428	13.982327	17.559467
68.744073	9.268999	12.943046	13.576913	17.064113
69.267959	8.9893642	12.556197	13.171992	16.568468
69.795505	8.7104086	12.169977	12.767665	16.072667
70.326642	8.4322162	11.784511	12.364065	15.576888
70.861332	8.1548523	11.399901	11.9613	15.081275
71.399498	7.8784042	11.016278	11.559508	14.586015
71.941098	7.6029405	10.633748	11.158801	14.091259
72.486048	7.3285512	10.252445	10.759324	13.597201
73.034298	7.055308	9.8724817	10.361192	13.104003
73.585757	6.7833035	9.4939964	9.9645553	12.611862
74.140372	6.5126122	9.1171035	9.5695335	12.120948
74.698054	6.243324	8.7419396	9.176272	11.631458
75.258712	5.9755301	8.3686428	8.7849169	11.143591
75.822282	5.7093082	7.9973322	8.3955947	10.657524
76.388656	5.4447557	7.628155	8.0084617	10.17347
76.957765	5.1819522	7.261233	7.623647	9.6916089
77.529494	4.9209965	6.8967152	7.2413088	9.2121592
78.103769	4.6619691	6.5347251	6.8615782	8.7353041
78.680468	4.4049695	6.1754127	6.4846143	8.2612632
79.259509	4.1500802	5.8189037	6.1105507	7.7902241
79.840776	3.8973962	5.465342	5.7395401	7.3223989
80.424163	3.6470076	5.114864	5.3717274	6.8579904
81.009561	3.3990044	4.7676061	5.0072572	6.3972011
81.596859	3.1534761	4.4237037	4.6462736	5.940233
82.18594	2.9105129	4.0832935	4.2889216	5.4872895
82.776689	2.6702029	3.7465085	3.9353424	5.0385694
83.368984	2.4327688	3.4136047	3.585796	4.5944097
83.962707	2.1981988	3.0846235	3.2403352	4.1549064
84.557735	1.9664897	2.7596128	2.8990189	3.7201623
85.153942	1.737767	2.4387378	2.5620191	3.2904113
85.751203	1.5121226	2.1221311	2.2294759	2.8658499
86.34939	1.2896441	1.8099215	1.9015255	2.4466702
86.948375	1.0704149	1.502232	1.5782985	2.0330567
87.548029	0.8545167	1.1991831	1.2599226	1.6251911
88.14822	0.6420324	0.9008963	0.9465264	1.2232569
88.748819	0.4330475	0.6074947	0.6382401	0.8274433
89.349692	0.2276768	0.3191369	0.3352309	0.4380096

B. The results of new model the cylindrical nozzle with $d: \phi 30, l: 16mm$

Table B. The angular distribution by new model ($d: \phi 30, l: 16mm$)

Intensity

Angle [º]	0.08 g/h	0.313 g/h	0.94 g/h	1.566 g/h	3.13 g/h
0.1419618	100	100	100	100	100
0.7097958	99.656032	99.664534	99.682962	99.702701	99.758365
1.2774904	99.302361	99.318861	99.35469	99.393151	99.501993
1.8449345	98.939108	98.963109	99.015321	99.071497	99.231052
2.4120168	98.566403	98.597414	98.665003	98.737897	98.945721
2.9786256	98.184387	98.221922	98.303893	98.39252	98.646194
3.5446529	97.793204	97.836783	97.932156	98.035543	98.332675
4.1099884	97.393008	97.44216	97.549968	97.667155	98.005383
4.6745234	96.983962	97.038221	97.157512	97.287553	97.664548
5.2381502	96.566232	96.625142	96.754979	96.896946	97.310411
5.8007612	96.139996	96.203108	96.342572	96.495548	96.943225
6.362253	95.705432	95.772307	95.920495	96.083583	96.563252
6.9225206	95.262731	95.332937	95.488963	95.661283	96.170764
7.4814609	94.812084	94.885199	95.048198	95.228887	95.766045
8.0389729	94.353692	94.429303	94.598427	94.786643	95.349385
8.5949556	93.887759	93.965463	94.139885	94.334803	94.921085
9.1493134	93.414493	93.493897	93.672809	93.873626	94.48145
9.7019489	92.934107	93.014828	93.197445	93.403376	94.030796
10.252768	92.446818	92.528485	92.714042	92.924325	93.569444
10.801678	91.952849	92.035098	92.222853	92.436747	93.097722
11.348591	91.45242	91.534902	91.724132	91.940919	92.615959
11.893409	90.945769	91.028142	91.21815	91.437133	92.124501
12.436064	90.433106	90.515043	90.705153	90.925658	91.623675
12.976451	89.914686	89.995868	90.185427	90.406804	91.113844
13.51451	89.390719	89.470841	89.65922	89.88084	90.595336
14.050141	88.861463	88.940228	89.126822	89.348081	90.068523
14.583287	88.327132	88.404258	88.588483	88.8088	89.533736
15.113855	87.787983	87.863197	88.044497	88.263315	88.99135
15.641792	87.244232	87.317275	87.495113	87.711898	88.441697
16.167009	86.696138	86.76676	86.940626	87.154868	87.885155
16.689459	86.143915	86.211879	86.381285	86.592499	87.322054
17.209058	85.587821	85.652901	85.817385	86.025107	86.75277
17.725755	85.02808	85.090062	85.249183	85.452975	86.177644
18.2395	84.464915	84.523595	84.676936	84.876383	85.597014
18.750217	83.898579	83.953766	84.100935	84.295644	85.01125
19.257872	83.32928	83.380793	83.52142	83.711022	84.420674
19.762393	82.757269	82.80494	82.938677	83.122826	83.82565
20.263753	82.182748	82.226418	82.352941	82.531314	83.226494
20.761884	81.605964	81.645485	81.764493	81.936788	82.623561
21.256762	81.027114	81.06235	81.173562	81.339499	82.017158
21.748328	80.446438	80.477262	80.580421	80.739744	81.407634
22.236561	79.864126	79.890424	79.985292	80.137764	80.795283
22.721407	79.280413	79.302078	79.388441	79.533846	80.180444
23.20285	78.695481	78.712419	78.790081	78.928226	79.563401
23.680841	78.109557	78.121683	78.19047	78.321179	78.944482
24.155369	77.522818	77.530055	77.589812	77.712931	78.323959
24.626388	76.935481	76.937763	76.988356	77.103748	77.702146
25.093893	76.347715	76.344984	76.386296	76.493846	77.079304
25.557843	75.759729	75.751938	75.783871	75.88348	76.455733
26.018237	75.171682	75.158793	75.181266	75.272853	75.83168
26.475039	74.583776	74.565757	74.57871	74.662212	75.207432
26.928251	73.996161	73.972991	73.976377	74.051747	74.583222
27.37784	73.40903	73.380693	73.374485	73.441693	73.959324
27.823815	72.822522	72.789014	72.773198	72.832231	73.335954
28.266146	72.236822	72.198144	72.172724	72.223581	72.713373
28.704844	71.652062	71.608222	71.573216	71.615913	72.091783
29.139886	71.068414	71.019429	70.97487	71.009437	71.47143
29.571275	70.486013	70.431906	70.37784	70.404321	70.852514
29.999018	69.904988	69.845789	69.782277	69.800728	70.235229
30.423098	69.3255	69.261245	69.18836	69.19885	69.619797
30.84353	68.747657	68.678388	68.596215	68.598827	69.006385
31.260302	68.171609	68.097374	68.006013	68.000838	68.395201
31.673434	67.597455	67.518309	67.417867	67.405011	67.786398
32.082915	67.025337	66.94134	66.831938	66.811514	67.180169
32.488767	66.455346	66.366562	66.248331	66.220464	66.576654
32.890982	65.887613	65.794112	65.667193	65.632018	65.976031
33.289586	65.322221	65.224078	65.08862	65.04628	65.378426
33.684574	64.759292	64.656586	64.51275	64.463397	64.784005
34.075973	64.198901	64.091715	63.939668	63.883462	64.192878
34.46378	63.641161	63.529584	63.369503	63.306611	63.6052
34.848024	63.086139	62.970262	62.802329	62.732927	63.021069
35.228706	62.53394	62.413858	62.238266	62.162535	62.440624
35.605857	61.984622	61.860435	61.677381	61.595508	61.863952
35.979478	61.438284	61.310093	61.119781	61.031961	61.29118
36.349602	60.894975	60.762886	60.565526	60.471957	60.722385

36.716232	60.354787	60.218907	60.014715	59.915602	60.15768
37.079404	59.817761	59.678202	59.467399	59.36295	59.597129
37.439122	59.283982	59.140857	58.923668	58.814097	59.040838
37.795422	58.753486	58.60691	58.383565	58.269088	58.488859
38.148311	58.226348	58.076439	57.847173	57.72801	57.941286
38.497826	57.702599	57.549477	57.314526	57.190902	57.398161
38.843974	57.182308	57.026095	56.785701	56.65784	56.859568
39.186787	56.66551	56.506329	56.260735	56.128867	56.325552
39.526295	56.152236	55.990212	55.739665	55.60402	55.796154
39.862509	55.642547	55.477805	55.222554	55.083365	55.271442
40.195466	55.136458	54.969126	54.709422	54.566921	54.751438
40.525179	54.634023	54.464229	54.200324	54.054748	54.236201
40.851686	54.135253	53.963127	53.695275	53.546859	53.725745
41.175001	53.640197	53.465868	53.194324	53.043305	53.220122
41.495161	53.14886	52.972459	52.697479	52.544094	52.719337
41.812181	52.661287	52.482945	52.204786	52.049271	52.223433
42.1261	52.177479	51.997327	51.716245	51.558838	51.732412
42.436933	51.697475	51.515645	51.231897	51.072833	51.246309
42.744718	51.221272	51.037896	50.751739	50.591255	50.765117
43.049471	50.748905	50.564114	50.275805	50.114135	50.288867
43.351231	50.280368	50.094294	49.804088	49.641466	49.817545
43.650015	49.81569	49.628465	49.336618	49.173276	49.351175
43.945861	49.354863	49.166618	48.873383	48.709553	48.889741
44.238785	48.897913	48.708778	48.414408	48.250319	48.433258
44.528828	48.444827	48.254933	47.95968	47.795559	47.981706
44.816004	47.995627	47.805105	47.509218	47.345292	47.535096
45.015857	47.682689	47.491802	47.195619	47.031963	47.2246
45.310754	47.220453	47.029141	46.732742	46.569689	46.766942
45.608686	46.752921	46.561318	46.264974	46.102785	46.305235
45.909687	46.280054	46.088304	45.792301	45.631248	45.839502
46.213778	45.801846	45.610099	45.314737	45.155105	45.369795
46.520995	45.318262	45.126678	44.832274	44.674364	44.896146
46.831374	44.829275	44.638021	44.344909	44.189033	44.418592
47.144933	44.334887	44.14414	43.85267	43.699158	43.937202
47.461709	43.835077	43.645024	43.355563	43.204757	43.452023
47.781733	43.329837	43.140674	42.853609	42.705869	42.96312
48.105039	42.819156	42.63109	42.346823	42.202524	42.470551
48.431646	42.303055	42.116303	41.83526	41.694791	41.974412
48.761588	41.781534	41.596324	41.318948	41.182718	41.474775
49.094896	41.254609	41.071179	40.797935	40.666366	40.971733
49.431604	40.72229	40.540892	40.272264	40.145798	40.465372
49.771728	40.18463	40.005526	39.74202	39.621113	39.955818
50.115302	39.641655	39.465121	39.207265	39.092393	39.443177
50.462355	39.093414	38.919737	38.66808	38.559735	38.927571
50.81292	38.539955	38.369434	38.124548	38.02324	38.409123
51.167011	37.981366	37.814315	37.576795	37.483049	37.887996
51.52466	37.417721	37.254465	37.024927	36.939286	37.364331
51.885892	36.849112	36.689992	36.469074	36.392097	36.838292
52.250741	36.275639	36.121007	35.909371	35.841631	36.310042
52.619217	35.697452	35.547673	35.345999	35.288085	35.779788
52.991349	35.114683	34.970136	34.779128	34.73164	35.247715
53.367161	34.527499	34.388574	34.208953	34.172505	34.714034
53.746682	33.936077	33.803177	33.635682	33.610897	34.178957
54.129918	33.340653	33.214192	33.059578	33.047087	33.642742
54.516898	32.741459	32.62186	32.480897	32.481334	33.105629
54.907641	32.138772	32.026468	31.899933	31.913934	32.567883
55.302172	31.532892	31.428322	31.317001	31.345199	32.029777
55.700493	30.9242	30.827807	30.732485	30.775502	31.491629
56.102628	30.313089	30.225318	30.146774	30.20522	30.953746
56.5086	29.700009	29.621302	29.560303	29.634764	30.416452
56.918407	29.085513	29.016305	28.973595	29.064624	29.880126
57.332068	28.4702	28.410911	28.387198	28.495304	29.345136
57.749595	27.854774	27.805805	27.801746	27.92738	28.81189
58.171005	27.240048	27.201766	27.217947	27.361484	28.280812
58.596291	26.627014	26.599744	26.636654	26.798367	27.752399
59.025465	26.016821	26.000824	26.058823	26.238858	27.227158
59.458534	25.410877	25.406328	25.485604	25.683936	26.705671
59.895509	24.810924	24.817882	24.918389	25.134771	26.188597
60.336374	24.219252	24.237609	24.358976	24.592856	25.676759
60.781138	23.638938	23.668346	23.809737	24.060142	25.171187
61.229797	23.074613	23.114351	23.274218	23.539524	24.673396
61.682356	22.534859	22.583511	22.758983	23.03638	24.186253
62.138792	22.045846	22.099959	22.284299	22.567482	23.719074
62.599105	21.574276	21.63238	21.822751	22.109106	23.25664
63.063284	21.102719	21.164539	21.360415	21.649475	22.791969
63.531325	20.631244	20.696505	20.897369	21.188667	22.325143
64.003195	20.159947	20.228378	20.433717	20.726794	21.85628
64.478886	19.688901	19.760236	19.969543	20.263942	21.385473
64.958379	19.21819	19.292165	19.50494	19.80021	20.912828
65.44166	18.747894	18.82425	19.039998	19.335692	20.43845
65.928685	18.278152	18.356631	18.574861	18.870537	19.962488
66.419438	17.809029	17.889379	18.109611	18.404832	19.485046
66.913897	17.340581	17.422557	17.644319	17.938659	19.006222
67.412011	16.872939	16.956297	17.179126	17.472163	18.526174
67.913754	16.406196	16.490698	16.714138	17.005459	18.045026

68.419089	15.940458	16.02587	16.249474	16.538671	17.562919
68.927984	15.475823	15.561917	15.785244	16.071918	17.079988
69.440376	15.012418	15.09897	15.321593	15.605352	16.5964
69.956228	14.550348	14.637138	14.858635	15.139097	16.112299
70.475492	14.089725	14.17654	14.396503	14.673292	15.62784
70.998125	13.63066	13.717291	13.935317	14.20807	15.143176
71.524051	13.173288	13.259533	13.475233	13.743592	14.658491
72.053224	12.717723	12.803383	13.016378	13.279997	14.173943
72.585581	12.264089	12.348973	12.558893	12.817436	13.689706
73.12107	11.812502	11.896423	12.102911	12.356052	13.205945
73.659603	11.363107	11.445886	11.648596	11.896019	12.72286
74.20112	10.916027	10.997488	11.196084	11.437485	12.240623
74.745549	10.471391	10.551366	10.745527	10.98061	11.759419
75.292825	10.029325	10.107652	10.297064	10.525548	11.279429
75.842848	9.5899791	9.6665017	9.8508674	10.072481	10.80086
76.395547	9.1534811	9.2280493	9.4070812	9.6215649	10.323898
76.950839	8.7199674	8.7924374	8.965861	9.172967	9.8487374
77.508648	8.2895674	8.3598017	8.5273548	8.7268471	9.3755657
78.068863	7.8624359	7.9303034	8.0917366	8.2833918	8.9045999
78.631402	7.4387035	7.5040794	7.6591559	7.8427625	8.4360305
79.196176	7.0185055	7.0812714	7.229767	7.4051257	7.9700536
79.76308	6.6019869	6.6620309	6.8037342	6.9706584	7.5068768
80.332017	6.1892866	6.2465028	6.3812154	6.5395307	7.0467005
80.902886	5.780542	5.8348313	5.9623672	6.1119117	6.5897245
81.475581	5.3758935	5.4271629	5.5473492	5.6879734	6.1361516
82.049998	4.9754778	5.0236405	5.1363167	5.2678838	5.6861804
82.626029	4.5794329	4.6244086	4.7294269	4.8518121	5.2400111
83.203561	4.1878957	4.2296101	4.3268353	4.4399265	4.7978427
83.782485	3.8009998	3.8393847	3.9286938	4.0323909	4.3598695
84.362685	3.4188799	3.4538732	3.5351557	3.6293706	3.9262874
84.944048	3.0416663	3.0732118	3.1463689	3.2310258	3.4972865
85.526458	2.6694892	2.6975365	2.7624818	2.8375163	3.0730567
86.109793	2.3024768	2.3269814	2.3836397	2.4489994	2.6537844
86.693939	1.9407524	1.9616752	2.0099831	2.0656268	2.2396505
87.278773	1.5844394	1.601747	1.6416521	1.6875498	1.8308349
87.864175	1.2336546	1.2473189	1.2787801	1.3149128	1.42751
88.450024	0.8885123	0.8985105	0.9214975	0.9478573	1.0298453
89.036196	0.5491164	0.5554314	0.5699254	0.5865159	0.6380029
89.622571	0.2155217	0.2181447	0.2241438	0.2309854	0.2521236

C. The results of DSMC for the cylindrical nozzle with $d\!:\phi16, l\!:30mm$

Table C. The angular distribution by DSMC ($d\!:\phi16, l\!:30mm$)

Intensity

Angle [º]	0.167 g/h	0.831 g/h	0.96 g/h	1.68 g/h	2.786 g/h	3.82 g/h	5.35 g/h	8.9 g/h
0.142	95.8	96.9	97.9	100.2	100.2	100.2	100.2	100.2
0.709	98.415458	96.856047	97.308983	100.51613	100.82182	100.74603	100.74603	100.67582
1.276	98.53279	97.427813	98.439932	99.255978	100.76369	100.44047	100.44047	99.159278
1.843	95.997534	96.413076	96.629224	99.794702	99.146485	99.25028	99.25028	99.532365
2.410	93.787548	95.351897	94.899069	100.01741	98.779781	99.095013	99.095013	99.346649
2.976	92.931427	95.000126	96.078423	99.2872	98.327119	99.176866	99.176866	99.337911
3.541	92.180836	95.210827	94.911099	98.605637	98.326401	97.244608	97.244608	98.599526
4.106	90.083308	94.126619	93.668711	97.972131	98.51167	97.550154	97.550154	98.279706
4.670	88.814565	93.649364	93.463875	96.645471	97.070706	97.959167	97.959167	97.470404
5.233	87.532645	92.941782	92.234002	98.38943	97.696684	97.045941	97.045941	97.583871
5.795	88.189761	91.638486	92.733911	96.860024	96.202385	96.828682	96.828682	96.791465
6.356	87.422336	91.071499	92.682794	95.517729	96.657602	96.24587	96.24587	96.629468
6.916	82.529154	89.791462	92.05689	95.499986	94.894159	95.044775	95.044775	96.612808
7.474	84.528124	88.321149	91.856299	95.11169	95.543884	95.197494	95.197494	95.617604
8.031	81.374644	87.782689	90.309441	94.422147	95.840388	95.529475	95.529475	95.122836
8.587	82.193536	87.380294	88.50904	94.31642	93.412267	94.221036	94.221036	94.934588
9.140	80.776472	86.480893	88.492245	93.502825	93.712445	93.903941	93.903941	93.158091
9.693	78.545376	86.947221	88.189759	93.178382	92.539626	93.209368	93.209368	93.590419
10.243	77.68736	85.345716	88.965013	92.658551	92.664391	92.042372	92.042372	93.484694
10.791	76.332729	84.658118	86.570241	92.665035	92.661313	93.176117	93.176117	92.292738
11.338	74.714632	84.776984	86.24706	91.72822	91.559354	91.42117	91.42117	90.623246
11.882	71.875996	83.308617	85.394772	90.742057	90.729836	91.152007	91.152007	90.764413
12.424	71.696867	81.677003	84.079187	89.938068	90.936123	90.890126	90.890126	89.665589
12.964	71.276044	82.143395	83.989735	89.764462	89.505128	88.763553	88.763553	88.896034
13.502	72.879113	81.448999	82.15444	88.94222	88.892386	88.934354	88.934354	88.658128
14.037	70.082587	80.355353	82.774044	89.609594	88.837137	88.51971	88.51971	88.449927
14.570	70.700364	79.143609	80.7774	87.204884	87.440356	86.900723	86.900723	86.83761
15.100	69.154145	77.981453	81.162475	87.225946	85.693484	86.492933	86.492933	86.312969
15.627	69.893814	77.207616	79.102082	86.685463	84.76086	86.359458	86.359458	87.276931
16.152	65.097768	76.257164	78.688502	85.518449	84.978746	85.447891	85.447891	85.541939
16.674	64.834484	75.513104	78.448641	85.053731	84.26587	85.953204	85.953204	84.961912
17.193	67.062552	74.439628	77.149629	83.717518	82.890768	84.067846	84.067846	84.537211
17.709	64.067464	73.834823	76.703765	82.639312	83.640937	83.564465	83.564465	83.742362
18.223	62.364972	73.535626	74.160685	83.42624	81.326316	82.324146	82.324146	82.665664
18.733	60.918494	71.79097	73.755772	81.807696	83.216486	81.664661	81.664661	82.182205
19.240	61.336359	71.663243	73.701112	80.781085	81.214442	81.077042	81.077042	81.448174
19.745	59.189812	70.57247	72.750108	79.96382	83.027168	80.728602	80.728602	79.981274
20.245	57.925809	69.412254	72.946011	80.065655	80.145513	79.653378	79.653378	79.788826
20.743	56.02103	68.89644	72.039181	78.865856	78.950557	78.865691	78.865691	78.636104
21.238	57.200818	68.587566	72.259151	77.289796	78.970295	78.395749	78.395749	78.900925
21.729	55.44208	67.748029	70.432244	76.693985	78.717714	77.061387	77.061387	78.611621
22.217	55.37514	67.500361	69.610185	76.652631	76.898963	76.972511	76.972511	76.910699
22.701	52.77108	66.485285	69.647636	76.70357	76.920826	76.205282	76.205282	76.212745
23.182	53.103708	64.507042	67.456046	74.527766	75.769133	75.632004	75.632004	76.03555
23.660	52.585907	64.684546	65.139063	74.840505	74.523086	75.297566	75.297566	74.541232
24.134	51.530933	62.876274	64.053923	73.365919	73.722293	73.996693	73.996693	72.908388
24.605	51.314376	63.530084	63.642658	72.582491	72.127134	72.799819	72.799819	72.856362
25.072	48.719792	62.241821	62.15261	72.068086	72.14395	73.403582	73.403582	72.055744
25.536	47.740471	60.887685	60.748561	70.814005	73.423128	71.436305	71.436305	70.922921
25.996	48.282255	59.763108	62.487279	69.959773	71.988809	71.485481	71.485481	70.17334
26.453	47.333162	58.990511	62.779946	69.269895	70.07811	70.534026	70.534026	69.105632
26.906	47.089672	58.38189	60.079133	68.368385	70.816324	68.660553	68.660553	69.000842
27.355	45.23154	58.255405	59.879976	67.84409	69.858397	69.575799	69.575799	68.579764
27.801	43.992474	57.534291	58.808163	67.360839	68.326035	67.81107	67.81107	67.522595
28.243	42.598649	55.966259	58.999223	65.979859	66.917067	67.297739	67.297739	66.147816
28.681	42.648326	55.873746	58.793116	65.519802	66.319278	66.757631	66.757631	66.683455
29.116	42.543776	54.227005	57.21653	66.024612	64.183035	65.842362	65.842362	65.168518
29.547	41.343108	53.898557	55.890807	64.824585	64.87897	63.031781	63.031781	65.00139
29.975	41.366056	53.628673	54.120976	63.573415	65.614318	64.370381	64.370381	63.169649
30.399	41.471451	52.117433	53.286381	62.892593	63.025099	63.103938	63.103938	63.663013
30.819	39.315847	51.479124	52.980296	62.503012	62.323404	61.991048	61.991048	63.053144
31.235	39.436575	51.157152	53.076779	62.267626	61.515716	62.251945	62.251945	62.678305
31.648	39.444173	51.338867	52.172391	61.520361	61.237027	60.813527	60.813527	61.882036
32.058	38.672596	50.961988	52.105295	61.149827	61.524014	60.725224	60.725224	60.676583
32.463	38.594661	50.186693	53.11944	59.081539	58.931027	60.560859	60.560859	59.600418
32.865	36.399221	49.401059	51.792225	58.188655	59.219146	60.000076	60.000076	57.941942
33.264	36.343909	49.006834	51.154926	57.374001	57.949833	59.209796	59.209796	57.247834
33.659	38.874161	49.113097	49.676433	57.079049	59.426932	57.791291	57.791291	57.386492
34.050	35.74363	47.958988	50.131157	56.165487	58.805217	55.942393	55.942393	56.272071
34.438	35.417043	47.918238	48.242325	56.125411	58.470086	56.528095	56.528095	56.257595
34.822	35.761798	46.994989	47.507141	55.909612	56.421742	56.593388	56.593388	55.064139
35.202	33.711771	45.937965	47.157429	55.152172	53.750274	55.919089	55.919089	54.308105
35.579	33.536871	45.249333	45.188999	54.758317	55.073091	55.516266	55.516266	53.899994
35.953	33.608725	45.677402	47.133626	54.208647	54.164758	52.886583	52.886583	53.870165

36.323	33.341403	43.991779	47.396179	53.262172	53.763599	53.335592	53.335592	53.071095
36.689	33.677221	43.693769	45.263419	52.187888	53.658767	53.156132	53.156132	52.05867
37.052	32.88222	43.885863	43.510048	52.303678	53.015822	52.922898	52.922898	50.986355
37.412	31.93483	42.487066	43.130373	51.435048	52.934481	53.085685	53.085685	51.039909
37.768	31.37244	42.15657	43.407799	50.598507	51.829529	52.943294	52.943294	51.902852
38.121	31.767742	42.523843	42.112796	50.434413	51.120852	51.217072	51.217072	50.550144
38.470	30.971357	41.708801	43.030194	48.606343	49.896848	50.720637	50.720637	50.254414
38.817	30.268977	41.530753	42.69723	49.077042	50.117855	50.431211	50.431211	49.444836
39.159	29.684584	42.475213	42.399095	48.345537	49.716512	48.922968	48.922968	48.702833
39.499	31.469102	40.874032	42.530471	48.382187	49.386722	49.741938	49.741938	47.579319
39.835	30.076798	39.841897	41.362204	48.257632	48.646671	49.017221	49.017221	48.520596
40.168	29.794947	39.593661	40.096747	47.24849	49.347453	48.248108	48.248108	47.367763
40.497	29.511484	38.846947	40.333481	46.881311	48.510082	47.857016	47.857016	46.241049
40.824	29.769044	37.656474	40.353968	45.691945	47.200153	47.613397	47.613397	46.571915
41.147	28.019345	38.297223	39.492306	46.468614	48.394327	46.857725	46.857725	45.73226
41.467	27.488746	37.844028	39.209038	46.144103	47.039549	45.641046	45.641046	45.32235
41.784	27.277609	37.437301	38.034497	46.15295	46.13356	45.871099	45.871099	45.401426
42.098	27.023362	37.855202	38.929806	44.51159	44.780113	45.284854	45.284854	44.688635
42.409	26.28441	36.132527	38.844784	44.185894	44.398124	44.438217	44.438217	43.591612
42.717	27.11358	35.415948	38.257817	43.95506	43.565029	43.827946	43.827946	43.30746
43.021	26.052495	35.684245	37.014808	43.752894	44.811346	44.005572	44.005572	43.437636
43.323	26.922912	35.277231	37.765647	43.481252	43.152514	42.976108	42.976108	42.766851
43.622	27.098725	34.990972	36.968653	42.894205	42.576953	42.65469	42.65469	42.742303
43.918	26.444254	34.721403	35.736164	42.680119	42.134548	42.180307	42.180307	41.506289
44.211	25.708421	34.801566	34.747901	41.642994	42.070699	42.34083	42.34083	41.134588
44.501	26.128593	33.73101	34.506989	42.560066	42.040186	42.351373	42.351373	41.126383
44.788	24.934068	32.813422	34.53179	41.282472	42.345036	41.502521	41.502521	40.155955
45.074	24.903977	32.469889	33.803926	40.01735	41.24869	42.071516	40.893292	40.12448
45.377	24.704038	33.4799	34.087948	40.121226	40.038013	41.629015	41.446442	40.201692
45.683	23.869828	33.590832	32.359111	39.612467	40.811758	40.622572	40.969299	39.668075
45.992	24.961578	32.281408	32.506366	40.795148	39.30269	39.200272	39.377255	38.701165
46.305	23.085429	32.32621	32.173745	39.764988	40.179073	40.347699	40.007191	38.490189
46.620	22.705056	32.013765	32.233653	39.07488	38.836904	40.027955	39.363636	38.540216
46.940	22.8301	32.209559	33.292508	38.724423	38.765273	38.980393	39.14318	38.442081
47.262	21.733566	31.760138	32.485804	37.680563	38.90064	37.585274	39.20558	38.724138
47.588	21.777897	30.609415	31.922581	38.071974	38.113804	37.991503	38.043584	38.45102
47.917	22.178926	29.980534	32.318553	37.232081	37.416687	37.903617	37.070547	37.076034
48.250	23.034246	30.544912	30.698333	37.078247	37.569095	36.707829	37.107732	36.130091
48.586	20.782024	29.150805	30.150258	37.106299	37.332705	36.737242	36.218008	36.678538
48.926	21.532822	28.99479	30.954221	36.145971	36.669902	36.60461	36.019072	36.118637
49.270	22.246268	28.715427	30.959333	35.58036	35.314279	36.381305	35.948446	35.132991
49.617	21.633429	28.939361	29.408224	34.704699	35.109142	35.827697	35.144531	35.012658
49.967	21.991839	27.768391	28.156128	34.24101	34.359647	34.87089	34.772436	34.128272
50.321	21.377038	27.11844	29.229327	33.87077	33.791042	33.982312	34.69203	33.532869
50.679	20.941982	27.519	27.990969	34.097884	33.943813	33.765629	34.472036	32.353627
51.041	20.199074	26.910723	29.119875	32.826105	32.898452	33.769731	33.034977	32.805735
51.406	19.592572	27.395744	28.03243	32.425933	32.075996	33.761598	33.099369	32.950197
51.775	19.546457	26.454316	26.835089	32.769077	33.097971	32.538499	32.675719	32.643923
52.148	19.439613	25.174739	27.81532	31.6862	32.439982	32.099109	32.340149	31.671903
52.525	19.08916	26.006486	27.090405	32.096006	31.417831	32.045129	31.972769	31.499083
52.905	19.722316	25.452935	25.793621	31.887142	32.079347	31.606965	31.806021	30.546783
53.289	19.061642	24.691753	26.100431	30.817492	31.781528	30.62811	30.26348	30.00839
53.678	18.642544	24.015233	25.454568	29.839702	31.136987	30.747588	30.379369	29.695314
54.070	18.282624	23.137824	25.5493	29.867822	30.143895	30.492183	29.225478	29.345968
54.466	17.464409	23.949044	24.69078	29.723761	29.336229	29.091805	30.169201	28.578522
54.866	17.625075	23.216449	24.350118	28.813114	28.811853	28.790424	28.950724	28.175761
55.270	17.605635	23.649243	23.905712	27.909816	28.705109	28.412004	28.342937	27.943222
55.678	17.117852	22.706197	24.621925	27.786608	28.552183	28.039938	28.442555	26.831049
56.090	16.677345	22.078341	22.553426	27.331944	27.952614	27.733935	27.867987	26.699735
56.506	16.900344	21.993355	23.30916	27.819961	27.425573	26.922166	27.600816	26.30885
56.926	16.490523	20.639629	22.944454	26.84087	26.994147	26.948602	27.219112	26.112456
57.350	15.299963	20.719391	21.793804	26.884713	26.351112	26.061857	26.81966	25.266261
57.778	15.17664	20.396236	22.298262	26.746713	26.238992	25.887513	25.545669	24.7238
58.210	15.185669	20.452517	22.003427	25.560327	25.637577	24.982051	25.00638	25.0243
58.646	14.958444	20.093495	21.328058	25.233464	24.401495	24.43927	24.759743	24.587699
59.087	14.286933	19.766393	21.423187	24.317209	24.562425	24.559444	24.478032	23.937439
59.531	14.623197	18.989074	20.16173	24.059019	24.571412	23.602365	23.504947	23.424263
59.980	14.356017	18.475098	19.468281	23.977356	23.749131	24.164455	23.235363	23.122384
60.432	13.788508	18.071755	19.728815	23.427329	22.546428	23.205692	22.757731	22.514581
60.889	13.684073	18.467945	18.72949	22.616729	23.186284	22.43891	22.229775	21.912977
61.350	13.091371	17.850533	18.1085	22.228746	22.565756	21.903042	21.550238	21.342165
61.815	12.758759	17.216888	17.450682	21.631964	21.874553	21.371655	21.4059	21.438868
62.284	12.829979	17.206641	17.522118	21.288521	21.350061	21.268875	21.046172	20.722033
62.757	12.449005	16.309212	16.710088	20.391113	20.366974	20.591872	20.725703	20.179735
63.234	12.327274	16.085388	16.583892	20.270783	19.56174	20.041228	19.934711	19.803271
63.715	12.247131	15.607441	16.27776	19.876122	19.714045	19.490488	19.704163	19.345448
64.200	11.693703	15.050134	15.746291	19.371296	18.668955	19.298076	18.81325	18.791772
64.690	11.443736	15.276498	15.447014	18.708146	18.665675	18.888064	18.15107	18.356106
65.183	10.792961	14.773741	15.552711	18.41531	18.832134	18.628155	17.985371	17.925839
65.680	10.176688	14.049742	15.11908	17.755695	17.249733	17.958423	17.48913	17.173354
66.181	10.388324	14.124738	14.462058	17.849963	16.973454	17.548282	17.217151	17.148901
66.686	9.9161345	13.220582	13.689609	16.777205	16.580091	16.88295	16.762903	16.391425
67.195	9.8666306	13.018712	13.171424	16.651204	16.343577	16.355076	16.263316	15.923662
67.707	9.4400642	12.673098	13.269552	15.688958	16.027097	15.983894	15.825307	15.630391
68.224	9.4451763	12.335686	12.950156	15.416698	15.415502	15.167754	15.16133	15.349461

68.744	8.9523971	12.42591	12.205646	14.902042	14.529419	14.997646	14.811958	14.609218
69.268	8.5019928	11.582537	11.988273	14.567193	14.525601	14.453051	14.83186	14.217263
69.796	8.3228584	11.098202	11.465909	13.758362	14.059222	14.066092	13.491676	13.325771
70.327	8.3823862	10.921567	11.84648	13.813395	13.607583	13.790369	13.478146	13.480364
70.861	7.9984135	10.435144	11.53882	13.051893	12.968321	13.158647	13.138527	12.966127
71.399	7.9502368	9.8148558	10.408157	12.632068	12.660308	12.816455	12.979073	12.422607
71.941	7.530964	9.8142728	9.8568033	12.556266	12.13192	12.4108	12.1031	12.184725
72.486	6.945649	9.4867193	9.9660848	12.198025	11.583005	11.52016	11.904014	11.671197
73.034	7.0975476	8.9136858	9.8138035	11.667437	11.41661	11.360367	11.381346	11.392511
73.586	6.7785561	8.5769878	8.4668938	11.100292	11.084358	11.245881	10.889637	10.822868
74.140	6.2994665	8.4491959	8.1046638	10.420294	10.404991	10.402389	10.679329	10.439951
74.698	5.91438	8.0293508	8.7768489	10.126479	9.9274515	10.116651	9.756114	10.244492
75.259	6.442108	7.7883486	7.6716125	10.054773	9.7846677	9.795577	9.1415832	9.4335079
75.822	5.6630633	7.2064422	7.2280642	9.5384777	9.1488608	9.0503674	9.1723985	8.9979812
76.389	5.1055091	6.8944701	7.070174	8.809292	9.0329604	8.5729906	8.4485032	8.7980389
76.958	5.154566	6.5587276	6.3850635	8.5353379	8.3325846	8.4590591	8.2114483	8.3844984
77.529	4.8097867	6.3893964	6.538844	8.1195152	7.9894463	7.9284047	7.9633346	7.8460289
78.104	4.5181866	6.0672319	5.9024423	7.3192626	7.6166906	7.6265273	7.577193	7.7641029
78.680	4.2141917	5.7401851	6.4805283	7.2831942	7.2171882	7.3779848	7.1870456	7.0629675
79.260	4.0124752	5.3298436	5.9499517	6.6431797	7.098246	7.0124873	6.8974508	6.7253353
79.841	3.8466999	4.9607917	5.5862126	6.5167203	6.5862963	6.3358382	6.5839422	6.301323
80.424	3.8162941	4.5203411	4.8910119	5.9508602	5.9099163	6.2554386	6.2497214	6.1113073
81.010	3.3112846	4.2193602	4.6762323	5.6787515	5.7722105	5.6858728	5.8079215	5.5791868
81.597	3.0118743	3.9378867	4.335314	5.2525091	5.4600378	5.3718749	5.193121	5.379217
82.186	2.7614161	3.829829	4.0836096	4.7883213	4.8461343	4.8796656	4.97228	4.8885628
82.777	2.3996694	3.7406103	3.5986242	4.6434929	4.3629909	4.5358796	4.6960572	4.439097
83.369	2.2563514	3.2220133	3.1559383	4.4281096	4.2120738	4.2937862	4.252088	4.450499
83.963	2.1228753	2.8499487	2.9037316	3.7282299	3.6450954	4.0079575	4.0198755	3.7325643
84.558	1.8542797	2.7521382	2.6204329	3.332227	3.0794601	3.60853	3.5804213	3.5236614
85.154	1.5594985	2.2168691	2.4261324	2.9981883	3.4073686	2.9993312	3.2583243	3.1663863
85.751	1.5495262	2.0672173	2.0317124	2.7488436	2.8081249	2.6143125	2.7544097	2.9725936
86.349	1.322213	1.949423	1.9496282	2.3065551	2.4577378	2.553046	2.5176873	2.7389643
86.948	1.0536752	1.6777203	1.5938663	1.9345124	2.0688834	2.1515811	2.1901516	2.4184813
87.548	0.809545	1.4028691	1.4767072	1.5983837	2.0020925	1.9473232	2.0288347	1.9103117
88.148	0.6300706	0.9076814	1.0583115	1.4515196	1.5973441	1.8357688	1.4937153	1.4851815
88.749	0.502978	0.775919	0.9146821	1.1571714	1.3955933	1.4473778	1.3545084	1.3276769
89.350	0.2481222	0.5388285	0.6853072	0.7930511	0.8296092	0.9499613	0.990384	1.2257753

D. The results of DSMC for the cylindrical nozzle with $\boldsymbol{d: \phi 30, l: 16mm}$

Table D. The angular distribution by DSMC ($\boldsymbol{d: \phi 30, l: 16mm}$)

Intensity

Angle [º]	0.08 g/h	0.313 g/h	0.94 g/h	1.566 g/h	3.13 g/h	4.7 g/h
0.142	100	101.3	100.6	101.8	101.8	101.8
0.710	100.83588	99.476129	99.823024	101.02292	100.62119	101.71003
1.277	100.5191	99.5485909	98.436796	99.273862	101.18019	101.65233
1.845	98.546363	99.7318285	98.625648	99.995894	99.206019	101.59533
2.412	96.426443	98.2408889	99.028963	99.095994	100.63707	100.78112
2.979	94.695436	98.104887	97.870286	99.775989	99.985349	100.35657
3.545	96.306467	99.4423114	98.35977	99.57244	100.60204	99.975662
4.110	97.540798	100.064201	100.63816	98.127856	100.42007	100.41107
4.675	97.439743	97.8698515	99.147831	97.409863	99.979404	99.652453
5.238	95.828582	97.4583577	95.95764	98.377111	98.481032	98.902513
5.801	94.336428	95.4826846	95.604229	98.197211	99.34866	98.748652
6.362	92.078939	93.0303284	96.155845	97.829821	98.330643	98.470216
6.923	96.458292	91.5993228	96.811873	97.843588	97.663752	97.910592
7.481	90.572519	95.5954231	96.860585	96.924233	97.252851	98.046924
8.039	90.94004	97.1193151	95.542525	95.871725	97.526539	96.653626
8.595	93.877986	93.0951188	95.054177	95.004019	97.515302	96.661952
9.149	96.397091	93.6782367	93.316459	94.361226	95.900827	96.119277
9.702	92.318243	94.4639623	94.56104	93.965987	95.812368	95.795971
10.253	91.604993	91.1640586	93.775805	94.202008	94.618848	95.425135
10.802	93.632178	95.3090885	93.363987	93.424411	94.089059	94.771194
11.349	88.441308	94.2400459	93.112765	92.989719	93.875485	94.923041
11.893	92.491713	88.6477828	92.16105	91.921713	94.227978	94.253579
12.436	90.213196	90.7529428	92.202371	92.617152	92.601587	92.931685
12.976	85.493345	93.9800297	91.170114	90.889206	92.403291	92.578284
13.515	93.743736	90.8798233	89.90038	90.957059	92.16316	92.571281
14.050	93.476133	90.1328128	90.040077	90.050258	92.533557	91.689241
14.583	88.390198	90.804165	88.446738	89.629684	91.129585	91.241157
15.114	87.368249	90.6233672	89.313836	89.036728	89.824717	90.072764
15.642	86.515042	86.0832448	88.953044	87.848169	89.421128	89.797603
16.167	87.873115	90.0907119	87.615012	87.776849	88.22977	89.454632
16.689	84.004019	86.0875076	87.049594	86.982247	88.577513	88.040858
17.209	87.018254	91.0196573	87.20458	87.81876	87.809346	87.881727
17.726	87.221232	88.9048052	87.335704	86.831558	88.092948	87.462826
18.240	84.76724	83.6219299	84.901894	86.899544	87.124651	86.306316
18.750	84.919335	84.0696661	84.327372	86.022105	86.107627	85.569484
19.258	81.420491	80.3338755	84.877171	84.814069	85.537391	85.042553
19.762	85.413155	83.1704552	83.240647	83.714541	84.900833	84.692985
20.264	82.011802	84.2978833	83.02546	82.90184	83.877746	83.802565
20.762	87.772587	81.3366537	83.009501	82.497885	83.57538	83.522506
21.257	83.025726	80.7846193	81.395346	81.792793	83.059237	83.58984
21.748	85.041861	80.2612685	82.427308	80.818551	82.520342	82.194075
22.237	81.112907	79.9470984	79.798209	80.734808	81.426681	81.116734
22.721	81.453056	80.9142098	78.744542	80.259343	81.524113	80.424065
23.203	80.11803	78.269142	78.526234	78.982858	80.942455	79.96237
23.681	83.801935	77.3725275	79.24753	78.304484	79.317851	79.856283
24.155	81.646538	76.547106	76.751377	77.642835	79.183203	79.209731
24.626	78.98815	75.6723124	77.496125	76.804196	78.589497	77.815647
25.094	73.091819	74.1275363	78.65999	75.251076	76.959887	77.253578
25.558	70.798184	74.2753013	77.878942	76.321209	76.004596	76.261555
26.018	69.314987	76.334728	77.112755	75.037123	76.474324	75.036041
26.475	70.445522	75.2542308	74.367602	74.687434	76.190799	74.88237
26.928	71.955749	73.2920077	75.322007	74.15377	74.700617	74.199656
27.378	71.726289	73.6703455	74.412579	74.088481	74.851334	73.296959
27.824	66.829713	72.9997159	73.071317	72.632734	74.482492	72.629101
28.266	68.463492	71.0261882	72.003528	72.006527	72.866234	72.409671
28.705	68.233106	69.1978035	70.765879	71.824886	72.278194	71.303986
29.140	69.201107	70.8921323	72.155414	70.319434	70.96698	70.656013
29.571	75.995298	71.0453711	70.050902	69.710418	70.967071	70.714847
29.999	69.769365	68.4557917	69.257367	69.688386	70.355401	69.574819
30.423	70.434853	69.2745914	66.912632	68.738229	69.944927	68.702769
30.844	69.702047	66.0247459	66.944971	68.543994	68.847907	67.868846
31.260	72.051022	66.0801173	66.614805	67.363899	68.335691	67.327377
31.673	67.994814	66.5130517	67.4493	67.02081	66.959484	67.214245
32.083	67.22691	65.7371626	66.732331	66.236633	66.643007	66.372906
32.489	67.224081	65.3695134	66.745768	65.243234	66.313998	65.412408
32.891	68.852866	66.1120794	65.888775	66.250136	65.12051	64.508116
33.290	64.934557	66.2047864	65.639872	65.814668	64.550232	63.835831
33.685	63.788596	69.2633221	64.121555	64.734541	64.245359	63.283039
34.076	62.875262	65.2304615	63.37339	63.740012	63.330592	62.268484
34.464	65.639282	63.8558784	62.853732	61.918126	63.254055	62.683967
34.848	61.218553	61.3451893	61.445919	62.408043	63.017667	61.478397
35.229	65.567126	60.3289655	61.805215	61.951126	61.437697	60.783939
35.606	65.162085	60.8076899	61.427586	61.542272	60.889936	59.922508
35.979	61.385068	59.3123844	60.558422	60.214949	60.379442	59.662352
36.350	59.425416	59.2624129	60.276262	59.880486	59.932417	59.204727

36.716	58.999104	56.7214206	59.344834	59.537448	59.122399	58.460779
37.079	59.981629	57.6669305	59.064118	58.436646	59.287265	57.917966
37.439	64.53179	58.0139452	59.677799	56.860492	57.488115	57.218089
37.795	60.236062	57.9152962	57.332424	57.23444	57.436862	56.372801
38.148	56.000838	57.7705893	56.140894	56.471407	56.768249	56.051886
38.498	54.234119	57.4207537	56.427341	56.567831	55.362828	55.090104
38.844	56.783427	59.8540493	56.548339	55.454327	54.81462	54.777733
39.187	59.108956	58.4929376	54.341799	55.991971	55.233085	53.609371
39.526	59.612226	55.1845481	55.144963	54.510513	54.653815	53.845695
39.863	58.417415	55.8560533	55.359277	55.169304	54.904306	53.43201
40.195	56.737257	53.8007089	56.274755	54.347493	53.923838	52.692749
40.525	52.322982	51.6660184	53.953945	54.016049	54.297831	52.320201
40.852	53.17633	53.4195411	52.628542	52.635915	52.797476	51.732984
41.175	50.432552	53.033496	52.068787	52.493965	51.126655	50.779009
41.495	51.684455	51.4119816	51.855689	51.590456	51.406957	50.029785
41.812	53.85988	51.0279275	51.556844	51.318089	51.521001	49.798237
42.126	57.071417	49.3465213	50.901285	51.70364	51.368952	49.039407
42.437	56.534864	50.385024	50.444802	49.778258	49.624925	48.786002
42.745	49.725347	52.3607416	49.642943	48.558673	48.623781	48.777017
43.049	48.86809	49.6272877	48.624932	48.996037	48.243108	48.066695
43.351	46.778529	50.8670174	48.390985	48.793229	48.075326	47.736438
43.650	48.49215	47.9531208	48.397533	47.848889	47.205898	46.83189
43.946	49.844216	46.826997	47.087805	47.607088	46.521654	46.674496
44.239	45.86254	49.0763645	45.820735	46.787882	46.409667	46.651162
44.529	49.490051	48.3679868	45.382518	45.718407	45.601539	45.90076
44.816	46.505921	47.0750995	46.183651	46.015392	45.179058	45.155431
45.016	47.26799	45.7602133	46.498094	46.38666	44.670057	44.451957
45.311	44.657603	46.5053929	45.380001	44.849169	44.837683	44.326467
45.609	43.327005	45.0626211	45.512484	44.437468	44.315943	44.196357
45.910	45.624117	45.8286935	44.135096	44.587112	43.475885	43.882406
46.214	42.925213	43.9242058	43.809076	44.009284	43.361795	43.198587
46.521	45.547648	47.6465297	44.17354	43.604479	43.98909	42.742974
46.831	45.393538	43.9910833	43.69193	42.212998	42.773637	41.910782
47.145	42.049819	45.1613074	43.0306	42.014323	41.688799	41.80518
47.462	42.334119	43.5991637	42.369079	40.989635	40.828656	41.555192
47.782	40.456328	43.3760354	41.950737	41.375739	40.980481	40.754851
48.105	40.453175	43.3119935	41.303763	40.916848	40.573587	40.059578
48.432	41.027411	41.9757	40.534076	40.321841	40.73871	39.988935
48.762	40.128215	41.0108186	40.087977	39.569055	40.674199	38.986284
49.095	41.541451	40.0912591	40.01729	38.982577	39.896781	38.219986
49.432	40.009529	40.1889993	39.562217	38.508531	38.897369	37.782552
49.772	41.150688	39.7206964	39.113191	38.290342	38.561115	37.825611
50.115	39.163945	38.8339771	38.609012	39.218257	37.445337	36.84711
50.462	40.374845	39.7099933	37.635088	37.618343	37.414474	36.559109
50.813	38.812581	37.0110693	37.272059	36.943942	36.912487	35.887234
51.167	36.645437	36.5100337	36.933523	36.639366	35.761613	35.07095
51.525	36.739514	35.6896497	36.000525	36.041131	35.588448	35.102873
51.886	35.979323	35.6811405	36.001802	34.691332	35.145326	34.655807
52.251	36.245412	34.8638228	34.974807	35.014991	34.132325	34.431851
52.619	35.944426	34.7936886	35.246101	34.079871	33.840217	33.328239
52.991	36.000776	35.044738	35.194279	33.420784	32.88637	32.505963
53.367	33.952972	34.7561453	33.81119	33.317381	32.773618	32.858042
53.747	32.538961	34.4109343	32.734402	32.505854	32.982511	32.292486
54.130	32.689944	33.8985979	32.184448	31.823511	32.176986	31.242371
54.517	31.452156	33.6913645	31.240043	31.357054	31.206601	31.055432
54.908	31.961916	31.7232745	30.461102	31.039144	30.666431	30.478817
55.302	32.744186	31.4281734	30.666302	30.170567	30.396136	29.927638
55.700	30.671209	30.4621493	30.391783	29.643492	29.748373	28.979528
56.103	29.518373	30.851526	29.511871	29.270663	29.29142	28.374896
56.509	29.35309	28.7598132	29.358304	28.81963	28.508537	27.662484
56.918	28.836268	28.1905591	28.383458	28.466558	27.846553	27.193498
57.332	28.490256	27.709952	27.426565	27.091689	27.640565	27.218397
57.750	26.61205	27.0213873	26.920497	26.53547	26.668161	26.641835
58.171	26.262673	26.8640509	26.318122	25.956912	27.039054	25.811714
58.596	26.060473	27.8210087	26.078255	25.715996	26.241895	25.674424
59.025	25.153594	25.4845134	25.081816	25.478831	25.205333	25.00176
59.459	24.781176	24.9821632	24.562764	24.252076	24.69505	24.44339
59.896	24.334142	24.2160574	24.735879	24.154318	24.37595	23.950801
60.336	23.891613	23.8290245	23.676219	23.663809	23.686497	23.248439
60.781	23.340827	23.2046609	22.891414	23.115764	23.454921	22.74223
61.230	23.124201	22.4948502	22.576289	22.377972	22.898751	22.505961
61.682	22.299249	22.2145517	22.10616	22.075852	22.49278	21.864349
62.139	21.770351	21.9667924	21.332108	20.981892	22.203601	21.662497
62.599	21.373354	21.2007689	21.02695	20.531646	21.617435	21.114887
63.063	20.928283	20.9004803	20.910642	20.017543	20.775293	20.470714
63.531	20.557206	20.3290925	20.492162	20.047572	20.167365	19.834595
64.003	19.93875	19.7082999	20.372975	19.582841	19.809042	19.323693
64.479	19.532463	19.1456673	19.176229	19.038426	19.426654	18.976379
64.958	18.945471	18.742131	18.349377	18.662651	18.975129	18.591037
65.442	18.501948	18.3262893	18.222406	18.45382	18.180473	18.278669
65.929	17.974526	17.8535817	17.867378	17.734847	18.361827	17.701081
66.419	17.515855	17.2266752	17.304278	17.527645	17.706066	17.283649
66.914	16.880392	16.8239819	16.392175	16.612932	17.503593	16.972189
67.412	16.597771	16.2360394	16.365174	16.324762	16.829094	16.3194
67.914	15.971628	15.9622243	15.687786	15.52685	15.849382	15.769703

68.419	15.522742	15.7069939	15.662222	15.436596	15.325328	15.639029
68.928	15.394326	14.8951486	15.164031	14.884591	15.128863	14.951378
69.440	14.660354	14.8057284	14.55823	14.731234	14.853523	14.687738
69.956	14.291277	14.2695581	14.05389	13.981525	14.288396	14.484897
70.475	13.716206	13.6502995	13.946741	13.670994	13.806581	13.622079
70.998	13.382044	13.271954	12.953614	12.767293	13.7389	12.991947
71.524	12.909306	12.8075613	12.493204	12.392306	13.137008	13.005428
72.053	12.705751	12.4548604	12.414255	11.938984	12.711262	12.573692
72.586	12.032393	12.1325047	11.92917	11.616887	12.053595	11.799827
73.121	11.473402	11.6019058	11.223751	11.271091	11.729336	11.471985
73.660	11.036374	11.0255763	10.710711	10.691614	11.497569	11.218976
74.201	10.713386	10.7217422	10.466499	10.543171	10.896018	10.870311
74.746	10.317427	10.1283808	10.204987	10.278551	10.422498	10.256235
75.293	10.028055	9.67438473	9.5623345	9.7282887	9.8837814	9.8736829
75.843	9.5219211	9.10187118	9.1023285	9.5566592	9.332589	9.4586134
76.396	9.0038861	8.83497666	8.4457772	8.9024466	9.2003572	9.047927
76.951	8.4930702	8.44378662	8.2952309	8.3821938	8.7104418	8.7642254
77.509	8.0914309	7.96915107	7.7995145	8.1477879	8.496202	8.1020137
78.069	7.7555318	7.54419311	7.6412718	7.7667468	8.0463948	7.8697308
78.631	7.3873513	7.16939542	7.0112376	7.3488713	7.3486496	7.4238453
79.196	7.0759872	6.83324133	6.8185156	6.8349632	7.1652749	7.0799044
79.763	6.4020071	6.42212058	6.4396061	6.3849104	6.7311264	6.6665357
80.332	5.9920358	5.99958821	6.1840389	6.0117645	6.545256	6.3269959
80.903	5.7273435	5.6277097	5.2935356	5.515804	6.0831131	5.8491163
81.476	5.189252	5.19210928	5.1315058	5.1417096	5.5828524	5.5779964
82.050	4.8484189	4.8297676	4.6740941	4.8653382	5.1376071	5.0416632
82.626	4.3939646	4.54771093	4.3690632	4.7468986	4.7719169	4.7496169
83.204	4.1627526	4.1182957	4.0691479	4.2570095	4.3257833	4.4948606
83.782	3.7548718	3.74245805	3.5513378	3.7639855	4.0413397	4.0885046
84.363	3.3504887	3.42164693	3.3344795	3.5045182	3.7071294	3.7315852
84.944	2.9614553	2.94115104	3.0451654	3.2576086	3.2301904	3.4556179
85.526	2.591309	2.63431404	2.621258	2.7690046	3.0758008	2.9346828
86.110	2.2468833	2.29141917	2.1973767	2.4080285	2.6539281	2.7392002
86.694	1.9447035	1.96090063	2.0920049	2.2379792	2.3831287	2.3862069
87.279	1.5702701	1.65935326	1.9769419	2.0121321	2.0176488	1.9770756
87.864	1.2070342	1.28857151	1.5442125	1.6985501	1.9603344	1.6771496
88.450	0.88423	0.9465269	1.0983811	1.2516139	1.321998	1.4774164
89.036	0.5664304	0.67859564	0.7850969	1.1840754	0.9538398	1.1186159
89.623	0.2239117	0.34800632	0.6130476	0.7871264	0.6891351	0.7943434

E. The results of Experiment for the cylindrical nozzle with $d{:}\,\phi 16, l{:}\,30mm$

Table E. The results of the thickness by Experiment ($d{:}\,\phi 16, l{:}\,30mm$)

Thickness [Å]

Position [mm]	$0.167g/h$, $3600s$	$0.831g/h$, $720s$	$2.786g/h$, $240s$
−430	224.839	249.776	310.01
−420	227.539	268.839	325.84
−410	236.632	275.881	340.1
−400	263.177	290.436	361.28
−390	275.212	310.205	374.29
−380	292.18	319.411	395.18
−370	310.937	341.44	412.39
−360	321.679	357.527	426.32
−350	339.066	373.481	448.77
−340	360.032	396.784	469.12
−330	379.228	420.294	492.91
−320	407.19	435.29	507.98
−310	436.052	460.804	525.18
−300	457.712	477.974	558.67
−290	481.927	502.252	578.12
−280	515.314	525.113	593.55
−270	544.508	552.38	616.73
−260	577.702	565.454	637.51
−250	604.829	592.275	653.28
−240	633.004	615.924	669.68
−230	659.447	637.34	686.23
−220	689.579	660.911	705.96
−210	720.056	676.846	722.23
−200	752.367	695.256	734.87
−190	775.642	718.376	745.85
−180	802.191	729.543	760.59
−170	832.855	744.503	771.81
−160	856.093	766.104	779.76
−150	875.937	776.495	785
−140	896.552	783.092	799.47
−130	918.233	794.35	805.64
−120	930.764	798.176	810.3
−110	910.57	791.131	802.92
−100	894.914	784.28	792.96
−90	874.358	771.819	782.93
−80	853.876	757.596	776.98
−70	827.931	742.285	769.84
−60	800.912	720.822	760.89
−50	769.836	707.097	745.73
−40	747.787	688.294	728.19
−30	715.863	670.574	712.78
−20	686.424	645.812	695.63
−10	657.637	623.195	679.91
0	625.502	599.392	663.59
10	590.015	573.048	646.73
20	558.278	559.508	628.61
30	523.391	539.555	606.51
40	499.677	513.867	579.17
50	475.677	491.368	561.48
60	451.085	470.111	538.75
70	420.595	448.274	516.77
80	396.28	425.069	498.41
90	376.198	409.087	486.73
100	353.275	384.123	458.27
110	329.303	363.259	436.36
120	315.024	346.161	415.3
130	297.74	328.465	402.96
140	275.976	314.575	381.34
150	264.581	305.892	362.17
160	254.239	285.059	348.15
170	232.301	273.998	332.36
180	217.802	255.965	314.35
190	213.508	245.108	298.01
200	193.886	229.008	284.03
210	184.567	215.208	275.51
220	177.713	202.91	257.04
230	175.596	200.454	247.38
240	158.011	187.705	238.68
250	144.534	174.571	225.53
260	143.823	165.842	211.59
270	134.704	160.237	192.46
280	128.44	152.646	185.53
290	113.154	141.971	182.58
300	113.064	135.16	173.27

310	100.7542	127.617	160.51
320	99.647	117.77	156.83
330	92.3676	108.193	147.51
340	90.491	103.997	140
350	84.4746	98.8718	132.96
360	78.9328	94.429	128.02
370	77.0232	90.608	120.87
380	62.2082	85.7191	119.13
390	57.5974	79.6177	110.68
400	57.6324	76.6699	105.11
410	55.4272	70.3851	93.06
420	54.7475	66.471	95.19
430	52.0238	63.9898	90.19

Bibliography

[1] S. V. Slyke, A. Pignata, D. Freeman, N. Redden, D. Waters, H. Kikuchi, T. Negishi, H. Kanno, Y. Nishio and M. Nakai, "27.2: Linear Source Deposition of Organic Layers for Full-Color OLED," in *SID*, 2002.

[2] E. Lee, "Simulation of the thin-film thickness distribution for an OLED thermal evaporation process," in *Vacuum*, 2009.

[3] S. Jun, M. Kim, S. Kim, M. Lee and E. Lee, "A Study on the Evaporation Process with Multiple Point-Sources," in *Electron. Mater. Lett.*, 2013.

[4] K. Nanbu, "Angular distributributions of molecular flux from orifices of varivous thickness," in *Vacuum*, 1985.

[5] L. I. Maissel and R. Glang, Handbook of Thin Film Technology, New York: McGraw-Hill, 1970.

[6] Z. Shiwei, H. Jin and Z. Zhijun, "Computer Simulation of positional beaming effect of molecular flow in straight cylindrical pipeline by Monte carlo Method," in *Computer Science and Information Technology*, 2008.

[7] G. A. Bird, Molecular Gas Dynamics and the Direct Simulation of Gas Flows, Oxford: Clarendon Press, 1994.

[8] F. J. Alexander and A. Garcia, "The direct simulation Monte Carlo method," in *Computers in Physics*, 1997.

[9] S. Adamson and J. F. McGilp, "Measurement of gas flux distributions from single capillaries using a modified, UHV-compatible ion gauge, and comparison with theory," in *Vacuum*, 1986.

[10] W. Steckelmacher, "A review of the molecular flow conductance for systems of tubes and componests and the measurement of pumping speed," in *Vacuum*, 1966.

[11] R. Feres and G. Yablonsky, "Knudsen's Cosine Law and Random Billiards," in *Chemical Engineering Science*, 2004.

[12] X. Yan and Y. Xu, "Chapter 2 Physical Fundamentals of Chemical Vapour Deposition," in *Chemical Vapour Deposition: An Integrated Engineering Design for Advanced Materials*, Springer Science & Business Media, 2010, pp. 29-71.

[13] E. H. Kennard, Kinetic theory of gases: with an introduction to statistical mechanics, the University of Michigan: McGraw-Hill, 1938.

[14] S. W. Zhang, G. Z. Ji and J. Han, "The positional and angular distribution of molecules flowing through Cylindrical tube in free molecular flow," in *Physics Procedia*, 2012.

[15] M. Lee, "Angular Distribution of Molecular flow from Nozzles in Thermal Evaporation Process," in *Seoul Natioal University*, Seoul, 2016.

[16] J. Mun, "Study on the prediction of thermal evaporated thin film profile in Roll-To-Roll process by Virtual Collision Direct Simulation Monte Carlo," in *Seoul Natioanl University*, Seoul, 2016.

[17] M. Brouard and C. Vallance, Tutorials in Molecular Reaction Dynamics, Royal Society of Chemistry, 2010.

[18] N. Dongari, Y. Zhang and J. M. Reese, "Molecular free path distribution in," in *J. Phys. D: Appl. Phys.*, 2011.

[19] J. C. Helmer, "Solution of Clausing's Integral Equation for Molecular Flow," in *Journal of Vacuum Science & Technology*, 1967.

[20] Pfeiffer Vacuum GmbH, The Vacuum Technology Book Volume II, Pfeiffer Vacuum GmbH, 2013.

[21] D. Halwidl, Development of an Effusive Molecular Beam Apparatus, Springer, 2016.

[22] G. S. d. Freitas Barbosa, K. Vissing and B. Mayer, "Creation and Evaluation of Construction Guidelines Using CFD for Low Pressure Plasma Gas Feed-in Systems to Homogenize the Precursor Gas Flow," in *Open Journal of Fluid Dynamics*, 2016.

[23] T. Einwohner and B. J. Alder, "Molecular Dynamics. VI. FreePath Distributions and Collision Rates for HardSphere and SquareWell Molecules," in *The Journal of Chemical Physics*, Livermore, 1968.

[24] D. W. Stops , "The mean free path of gas molecules in the transition régime," in *Journal of Physics D: Applied Physics*, London, 1970.

[25] C. Hilsum, "Flat-panel electronic displays: a triumph of physics, chemistry and engineering," in *Phil. Trans. R. Soc. A*, 2010.

[26] M. Cölle and W. Brütting, "Thermal, structural and photophysical properties of the organic semiconductor Alq3.," in *physica status solidi (a)*, 2004.

[27] "Wikipedia," Wikipedia, the free encyclopedia, 11 7 2017. [Online]. Available:https://en.wikipedia.org/wiki/Tris(8-hydroxyquinolinato)aluminium. [Accessed 17 10 2018].

[28] K. Nanbu and Y. Watanabe, "Thickness distribution of films fabricated by the molecular beam epitaxy technique," in *Vacuum*, 1986.

[29] C. P. Malhotra, R. L. Mahajan and W. S. Sampath, "High Knudsen Number Physical Vapor Deposition: Predicing Deposition Rates and Uniformity," in *Journal of Heat Transfer*, 2006.

[30] F. J. Alexander and A. L. Garcia, "The Direct Simulation Monte Carlo Method," in *Computers in Physics*, 1997.